SIAM J. APPL. MATH.
Vol. 52, No. 1, pp. 181-221, February 1992

011

ROTATING CHEMICAL WAVES IN THE GRAY–SCOTT MODEL*

W. W. FARR† AND M. GOLUBITSKY‡

Abstract. A set of reaction-diffusion equations is considered, known as the Gray–Scott model, defined on a circle, and the stability of rotating wave solutions formed via Hopf bifurcations that break the circular $O(2)$ symmetry is investigated. Using a hybrid numerical/analytical technique, center manifold/normal form reductions are performed to analyze symmetry-breaking Hopf bifurcations, degenerate Hopf bifurcations, and Hopf–Hopf mode interactions. It is found that stable rotating waves exist over broad ranges of parameter values and that the bifurcation behavior of this relatively simple model can be quite complex, e.g., two- and three-frequency motions exist.

Key words. Hopf bifurcation, $O(2)$ symmetry, reaction-diffusion equations, normal form reduction, rotating (traveling) waves, mode interactions, Gray–Scott model

AMS(MOS) subject classifications. 58F39, 58F36, 58F14, 35K57, 35B32

1. Introduction.

In this paper we study numerically degenerate Hopf bifurcations of a reaction-diffusion model posed on a circle,

$$u_t = Du_{\zeta\zeta} + f(u, \alpha), \tag{1.1}$$

where u is a 2π-periodic function of ζ with values in $\mathbf{R}^n$, D is a positive-definite diagonal matrix of diffusion coefficients, f is a nonlinear smooth function, and α is a vector of parameters. We are particularly interested in whether rotating wave solutions that appear when the Hopf bifurcation breaks the $O(2)$ symmetry [Ruelle, 1973], [Golubitsky and Stewart, 1985] can be stable. Our interest stems from the fact that stable rotating waves exhibiting striking symmetry have recently been found for the Belousov–Zhabotinskii reaction in an annular reactor [Noszticzius et al., 1987], to which our circle is a first crude approximation. (Details of the experiments are given in § 2 below.) Indeed, from our perspective, it is the existence of this $O(2)$ symmetry that makes the existence of rotating wave solutions likely. We note that in the experiments the rotating waves were not found arising from small amplitude, as if by Hopf bifurcation. Nevertheless, these waves could still be born via Hopf bifurcations as unstable rotating waves if we look at the solution structure of model equations describing this experiment.

Our goal is to show that Hopf bifurcations to rotating wave solutions can be expected to occur in *any* sufficiently realistic model of the B-Z reaction. Of course, these waves need not be stable at bifurcation and might only be observable at finite amplitude after a secondary bifurcation where stability is restored. In this paper we show numerically that both stable and unstable Hopf bifurcations to rotating waves do occur in one of the simplest models for autocatalytic reactions on the annulus—the Gray–Scott model. In addition, we show that in this model the unstable branches of rotating waves can regain stability through secondary bifurcations. It is important to note that the numerical techniques we have used can, in principle, be applied to any

* Received by the editors February 5, 1990; accepted for publication (in revised form) November 8, 1990. The research was supported in part by Texas Advanced Research Program grant ARP-1100, and by National Science Foundation/Defense Advanced Research Projects Agency grant DMS-8700897.

† Department of Mathematical Sciences, Worcester Polytechnic Institute, Worcester, Massachusetts 01609.

‡ Department of Mathematics, University of Houston, Houston, Texas 77204-3476.

of the more realistic models. Moreover, as these models all contain at least as many parameters and equations as the Gray–Scott model, it seems likely that they will contain a solution structure at least as complicated as the one we describe for the Gray–Scott model.

We present the results of these numerical calculations to suggest an alternative to the methods of excitable media [Tyson and Keener, 1988], [Maginu, 1985], [Feroe, 1986], [Ellphick, Meron, and Spiegel, 1990] for finding periodic solutions to reaction-diffusion equations. We are interested, in particular, in the structure of solution sets that should be common to all such systems of equations. In particular, the annular geometry forces the existence of $O(2)$ symmetry; and hence, the expectation of the existence of symmetry-breaking Hopf bifurcations to periodic solutions known as rotating waves. Since we consider the symmetry of the equations to be of paramount importance, we abstract the annulus to a circle. In the context of reaction-diffusion equations on the line with periodic boundary conditions (the circle), it is impossible to obtain rotating wave solutions from stable Hopf bifurcations with fewer than three equations. For this reason we have attempted our numerical calculations on a system with that minimum number of components: the Gray–Scott model.

The Gray–Scott model [Gray and Scott, 1983] is the simplest model consistent with chemical principles that is known to exhibit temporal oscillations in a continuous stirred reactor. The chemical mechanism for this autocatalytic model consists of the two reversible reactions

$$A+2B\to 3B, \qquad B\to C, \tag{1.2}$$

which form the core of models like the much-studied Brusselator. Though this model is too simple to hope to describe B-Z chemistry quantitatively, it mimics some of the behavior in a continuous stirred reactor [Scott and Farr, 1988]. Another positive feature of this model is that no species are assumed to be artificially held constant, i.e., the "pool chemical" assumption is not used.

The main mathematical technique in this paper is that of center manifold/normal form reduction. Because we consider degeneracies in the spirit of [Golubitsky and Roberts, 1987] and [Chossat, Golubitsky, and Keyfitz, 1986], we must deal with center manifolds of dimensions as large as six and normal forms computed out to as high as fifth order. The resulting calculations are formidable and beyond the reach of hand calculation, so we have adopted a hybrid approach: the bifurcation formulae are obtained analytically but evaluated numerically. Obtaining the correct formulae is usually a difficult and time-consuming task in itself, but with the aid of the results in [Cushman and Sanders, 1986] and [Elphick et al., 1987] we have devised a systematic procedure for doing so that is easily checked using elementary combinatorics. Details of this procedure, which should extend easily to other types of bifurcations, are found in the Appendix.

We note that a very similar hybrid procedure was used before in [Labouriau, 1985, 1989], [Farr, 1986], and [Farr and Aris, 1987] to analyze degenerate Hopf bifurcations in models described by ordinary differential equations without symmetry. One minor difference is that these earlier investigations used the Lyapunov–Schmidt reduction, as described in [Golubitsky and Langford, 1981].

As an aside, we note that an alternative route to performing center manifold/normal form calculations involves the use of symbolic manipulators such as MACSYMA or Maple. Several monographs are available that detail this approach, for example, [Rand and Armbruster, 1987]. Although the Maple package was used to check some of the calculations in § 4, we chose not to use it for the reduction calculations for the

following reasons. First, a bifurcation analysis must start with a basic solution whose properties and stability are known. In the case of a reaction-diffusion system on a circle, this basic solution is constant. However, for the (relatively simple) Gray–Scott model, this basic solution cannot be found analytically. Because of this, all of the subsequent calculations must of necessity be done numerically. Given this fact, a completely numerical code is likely to be much faster. Second, we are interested in developing methods that will be useful for analyzing more complicated models and domains. If anything, these extensions will involve considerably more in the way of numerical computation and tip the balance even further away from the type of problem suitable for symbolic manipulation packages. Finally, symmetry-breaking bifurcations, and especially interactions between symmetry-breaking modes, lead to center manifolds of relatively high dimension. This leads to bookkeeping difficulties, especially when higher-order terms are needed. The algorithmic approach detailed in the Appendix describes our attempts to minimize the amount of work that must be done to calculate the normal form up to some given order.

The organization of this paper is as follows. In § 2 we summarize the experimental results of [Noszticzius et al., 1987] that motivate our work, briefly state our results for the Gray–Scott model, and relate our work to that of earlier investigators. In § 3 background material on Hopf bifurcation and Hopf–Hopf mode interactions with $O(2)$ symmetry for systems of reaction-diffusion equations posed on a circle is presented, which covers the main issues and summarizes the needed results. The Gray–Scott model is described in § 4, where we consider steady-state solutions that are constant on the circle. A linear stability analysis of these solutions allows us to determine which types of bifurcations occur and to locate them precisely. Finally, in § 5 we present the results of our nonlinear analysis for this model. By calculating coefficients in the normal form corresponding to a bifurcation point and using the material in § 3, we are able to describe locally the stability of emerging solutions, for example, rotating waves. In particular, we describe regions of parameter space for which stable rotating waves appear via a primary Hopf bifurcation that breaks the $O(2)$ symmetry. By computing the normal form up to cubic order for a mode interaction between two Hopf bifurcations (one $O(2)$-invariant and one that breaks the $O(2)$ symmetry) as in [Chossat, Golubitsky, and Keyfitz, 1986] we find a second region where the primary bifurcation is to stable $O(2)$-invariant periodic solutions, but rotating waves issuing from a second Hopf bifurcation become stable via a secondary bifurcation. Thus we find two periodic solutions that are simultaneously stable. To our knowledge, this is the first time that the six-dimensional $O(2)$ Hopf–Hopf interaction has been implemented numerically. We also briefly describe additional degeneracies that appear in this model: some have been analyzed (degenerate Hopf bifurcation with $O(2)$ symmetry [Golubitsky and Roberts, 1987] and Takens–Bogdanov bifurcation with $O(2)$ symmetry [Dangelmayr and Knobloch, 1987]), while others ($O(2)$ Hopf-invariant limit point, Takens–Bogdanov-$O(2)$ Hopf), have not. The overall picture is considerably complicated when compared to the CSTR dynamics.

2. Motivation and summary. The Belousov–Zhabotinskii (hereafter B-Z) reaction first came to the attention of researchers as an example of a chemical system exhibiting spontaneous temporal oscillations in well-stirred closed (i.e., no mass transport across the boundaries) [Field and Burger, 1985] and continuous flow reactors [Field and Burger, 1985], [Maselko and Swinney, 1986]. The occurrence of spatial patterns and waves in unstirred reactors was also noted earlier [Winfree, 1972], and has been of considerable interest, e.g., [Field and Burger, 1985]. In this paper we are primarily

concerned with spatio-temporal pattern formation in unstirred vessels. The early experiments in this area were almost exclusively carried out in closed vessels, in which a chemical system inexorably relaxes to a spatially uniform, constant equilibrium state, so the patterns observed were really transients. More recent experiments have attempted to overcome this problem. For example, the reactor of [Tam et al., 1988], which allowed sustained spiral waves to be observed, is in the form of a thin disk of gel (to suppress bubble formation and convection), which is fed continuously from beneath by a network of capillary tubes that communicate with a stirred, continuously fed reservoir. The experiments we are most interested in, however, are those of [Noszticzius et al., 1987]. A schematic of their apparatus is shown in Fig. 1. It consisted of a thin annular ring of inert gel sandwiched between impermeable boundaries top and bottom. The inner and outer edges of the annulus are exposed to stirred reservoirs continuously fed with the two components of the B-Z reaction. One advantage of this reactor, over the disk reactor of [Tam et al., 1988] as far as analysis is concerned, is that no reaction occurs in the reservoirs.

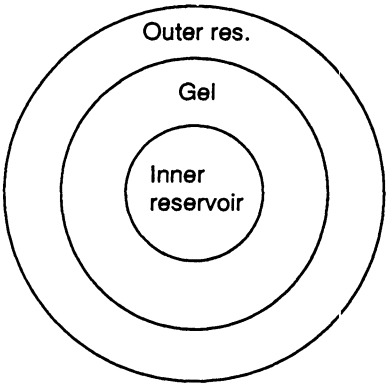

FIG. 1. *Schematic of annular gel reactor used by* [*Noszticzius et al.*, 1987].

We now describe the experimental results of [Noszticzius et al., 1987]. The outer reservoir contains the sulfuric acid and potassium bromate component, while the malonic acid and the ferroin catalyst are fed to the inner reservoir. When the reactor is started up, a circular front of ferroin advances from the inside. As it approaches the outer edge, the front becomes more irregular. Eventually, a state develops with several wave sources (pacemakers) distributed randomly around the outer edge, as illustrated in Fig. 2. The number of wave sources is irregular, as are their frequencies. The source for these pacemakers is not well understood, but they are thought to be related to local inhomogeneities, e.g., foreign objects, and it is thought that they can be removed by refining experimental techniques [Noszticzius et al., 1987]. It must be emphasized that these states are not accessible via the local bifurcation theory we will present in the next section. The experimenters, however, are able to perturb these states systematically and obtain stable rotating wave solutions similar to the one with eight wavefronts shown schematically in Fig. 2. They further state that the rotating waves are stable if the number of wavefronts lies between 6 and 25; below this range pacemakers appear spontaneously, and above it the waves interact destructively. From our point of view, the most striking feature of these states is their regularity and resultant high degree of symmetry. In fact, they possess spatio-temporal symmetry. This concept is best illustrated by example. Consider a state with eight equally spaced

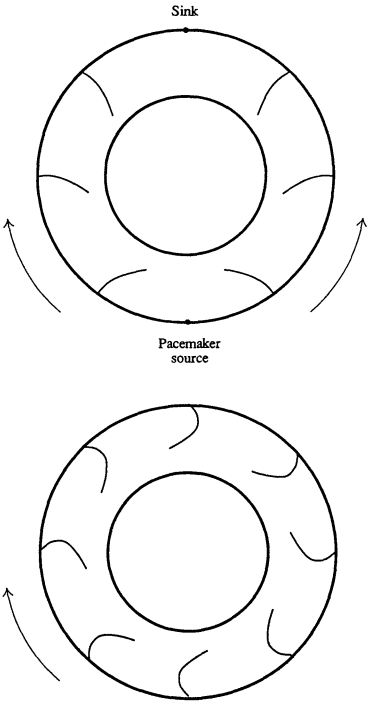

FIG. 2. *Top*: *single source and sink for pacemaker-induced chemical waves. Bottom*: *stable eight wavefront rotating wave.*

wavefronts. The state is periodic in time, but also in space: rotation of the solution through an angle of $2\pi/8$ is the same as letting the solution evolve through one temporal period.

Turning to the concept of symmetry, we consider the group $O(2)$ generated by the rotations and reflections in the plane. It turns out that, in a sense to be made precise in § 2, the reaction-diffusion equations are invariant under $O(2)$. We now describe how the experimental results of [Noszticzius et al., 1987] are consistent with a Hopf bifurcation that breaks that $O(2)$ symmetry. It is well known [Ruelle, 1973], [Schecter, 1976], [van Gils and Mallet-Paret, 1984] that two families of periodic solutions originate from such a point: standing waves and rotating waves. The first family will not be very important in this work, but the rotating waves are candidates for explaining the experimental results since they have the exact spatio-temporal symmetry described above.

To simplify the presentation and the calculations, we now consider reaction-diffusion equations defined on a circle as an approximation to a thin annulus. Such equations have the following form:

$$u_t = Du_{\zeta\zeta} + f(u, \alpha), \tag{2.1}$$

where u is a 2π-periodic function of ζ and has values in $\mathbf{R}^n$, D is a positive-definite diagonal matrix of diffusion coefficients, and α is a vector of parameters. The action of $O(2)$ on the circle is generated by

$$\begin{aligned} &\text{Rotation by } \psi\text{:} \quad \zeta \to \zeta + \psi \bmod 2\pi, \\ &\text{Reflection:} \quad \zeta \to -\zeta \bmod 2\pi \end{aligned} \tag{2.2}$$

and the action of $O(2)$ on the system of reaction diffusion equations is generated by

$$\begin{aligned} &\text{Rotation by } \psi: \quad u(\zeta) \to u(\zeta - \psi), \\ &\text{Reflection:} \quad u(\zeta) \to u(-\zeta). \end{aligned} \tag{2.3}$$

We want to use bifurcation theory to analyze (2.1); a first requirement is a solution from which to bifurcate. Note that we have not required the existence of a trivial solution to (2.1), and the model we consider does not have one. Their place in the theory, however, is taken by solutions that are invariant under the action of $O(2)$. Such solutions are easily seen to be constants, the solutions of the set of equations $f(u, \alpha) = 0$. The next step is to linearize (2.1) about one of these invariant solutions and decompose the stability analysis into an infinite sequence of finite-dimensional problems by using Fourier modes. That is, we consider linear stability of the invariant solution to disturbances of the form $v e^{im\psi} e^{\lambda t}$, where $v \in \mathbf{R}^n$ and $m = 0, \pm 1, \pm 2, \cdots$. The resulting finite-dimensional eigenvalue problem is

$$\lambda v = (A - m^2 D)v, \tag{2.4}$$

where A is the Jacobian of $f(u, \alpha)$ at the invariant state in question. It is clear from (2.4) that the eigenvalues for m are duplicated for $-m$. This is a direct result of the $O(2)$ symmetry. We call an invariant steady-state of (2.1) a bifurcation point if it has an eigenvalue with zero real part for at least one value of m. If $m \neq 0$ for one of the critical eigenvalues, we call the bifurcation point *symmetry-breaking*. We note that a decomposition into a direct sum of finite-dimensional subspaces is guaranteed by the theory of representations [Kirillov, 1976], but this decomposition is particularly convenient for calculations, as we will see below. We also note that since D is positive-definite the eigenvalues eventually have negative real parts for all sufficiently large m.

In most chemical systems of interest, the diffusion coefficients are nearly equal so the matrix D is close to a scalar multiple of the identity. If this is exactly true, then the eigenvalues of (2.4) for arbitrary m are related to those for $m = 0$ by translation, which can be seen easily by substituting $D = dI$ into (2.4). An important observation for our work on Hopf bifurcation is that, for equal diffusion coefficients, a symmetry-breaking Hopf bifurcation can never be the primary bifurcation point. This follows from (2.4) since, if there is a pure imaginary pair of eigenvalues for some $m > 0$, then there are complex conjugate pairs of eigenvalues with positive real part $(= n^2 d)$ for all n, $0 \leqq n \leqq m$. Thus to find stable rotating waves we must either have unequal diffusion or some mechanism by which the rotating waves can become stable when they are not the primary bifurcation. In our work with the Gray-Scott model, we encounter both of these cases.

We now briefly describe the Gray-Scott model and the results we have obtained. Technical details are given in §§ 3-5 and the Appendix. The model equations are

$$\begin{aligned} x_t &= D_1 x_{\zeta\zeta} - \beta x y^2 + \alpha_1 y^3 + \lambda(1 - x), \\ y_t &= D_2 y_{\zeta\zeta} + \beta x y^2 - \alpha_1 y^3 - y + \alpha_3 z + \lambda(\gamma_2 - y), \\ z_t &= D_3 z_{\zeta\zeta} + y - \alpha_3 z + \lambda(\gamma_3 - z) \end{aligned} \tag{2.5}$$

and are essentially those of [Balakotaiah, 1987] with diffusion terms added. The parameters appearing in (2.5) have physical meaning as follows: β represents a forward reaction rate coefficient, α_1 and α_3 are reverse reaction rate coefficients, λ represents a mass-transfer coefficient, and γ_2 and γ_3 are ratios of the feed concentrations of species B and C to that of species A. As described in [Balakotaiah, 1987], finding the

invariant solutions can be reduced to solving a single nonlinear equation that is cubic in y. Analytic solution is not possible, but the methods of [Golubitsky and Schaeffer, 1985] are used in [Balakotaiah, 1987] to classify all of the possible bifurcation diagrams for the invariant steady-states. For any particular parameter values the bifurcation diagram can be generated numerically using a standard path-following technique [Doedel, Jepson, and Keller, 1984].

Linear stability calculations must also be done numerically, and standard path-following techniques exist [Spence and Jepson, 1984]. Because the model is only three-dimensional, however, it is simpler to use the characteristic equation. Conditions for eigenvalues with zero real part can be formulated simply in terms of the characteristic equation coefficients and solving for particular configurations, for example, finding Hopf bifurcation points for a particular value of m, is relatively easy. However, to obtain local stability results from a center manifold/normal form reduction we really need information on all of the eigenvalues. This can be obtained as follows. We will show below that if λ is small enough, all of the eigenvalues have negative real parts. Hence, we can determine changes in stability simply by monitoring the signs of the conditions for eigenvalues with zero real part. In principle, we would have to do this for all values of m, but in practice we only have to monitor a finite number of modes because the eigenvalues eventually have negative real parts for large m.

Some typical results from the analysis are shown in Fig. 3. The parameter values were chosen so that there is a unique invariant steady-state and the only bifurcations occurring are Hopf bifurcations for $m=0$ and $m=1$. The invariant steady-state is initially stable. First, a pair of $m=0$ Hopf points appear and separate, then a pair of $m=1$ Hopf points appears between the $m=0$ Hopf points and, finally, the $m=1$ Hopf point at the smaller value of λ passes through the $m=0$ Hopf point and becomes the primary bifurcation point. The places where a pair of Hopf points appear are our first examples of degenerate Hopf bifurcation [Golubitsky and Langford, 1981], [Golubitsky

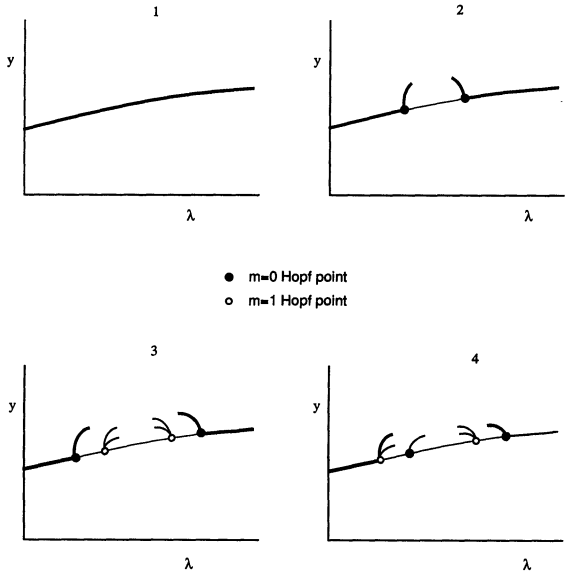

FIG. 3. *Typical linear stability results for Gray–Scott model.* (1) *Stable invariant steady-state.* (2) *Two $m=0$ Hopf points appear.* (3) *A pair of $m=1$ Hopf points appears.* (4) *The leftmost $m=1$ Hopf point becomes a primary bifurcation point by passing through the $m=0$ Hopf point. Main branch is steady-state; bifurcating branches correspond to periodic solutions.*

and Roberts, 1987], and the crossing of the $m=0$ and $m=1$ is a mode interaction [Chossat, Golubitsky, and Keyfitz, 1986]. By computing the normal form vector field for each Hopf point we can determine the local stability of the periodic branches, and this is also shown in Fig. 3.

By computing the six-dimensional normal form for the interaction of the $m=1$ and $m=0$ Hopf points up to cubic order and using the results in [Chossat, Golubitsky, and Keyfitz, 1986] we can obtain more information on how the stabilities change. Details are given below, but the local diagrams are as shown in Fig. 4. There we see that secondary bifurcations to quasi-periodic solutions (which are not stable) occur such that the rotating waves and the invariant periodic branch each become stable when they are not the primary bifurcation. One interesting result is that the rotating waves and the invariant periodic solutions are simultaneously stable.

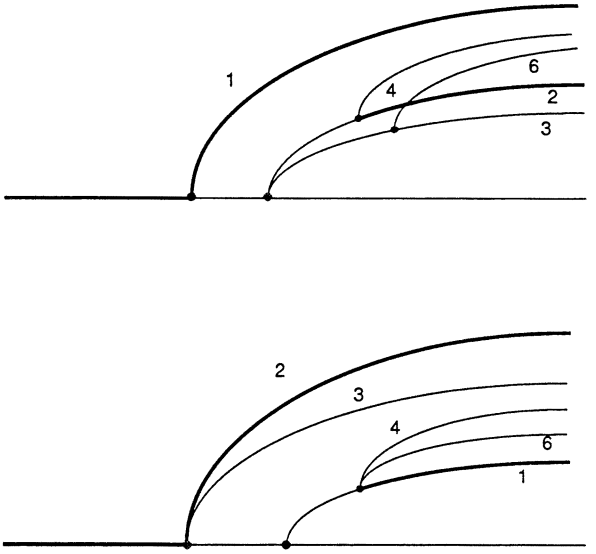

FIG. 4. *Sample local bifurcation diagrams for the six-dimensional* $m=0$, $m=1$ *Hopf–Hopf mode interaction. The branch of rotating waves is labeled* 2.

In § 5 we present more results by varying an additional parameter as well. It turns out that the sequence we have presented above holds in a fairly large region of parameter space, but we also encounter additional complications. For example, limit points can appear on the invariant steady-state branch via a hysteresis bifurcation. This leads to further complications in the form of Takens–Bogdanov singularities involving the invariant limit points and invariant Hopf points as well as interactions of the $m=1$ Hopf points with the invariant limit points. A codimension three singularity occurs when we have an invariant Takens–Bogdanov simultaneously with an $m=1$ Hopf point. By changing the values of the diffusion coefficients, Hopf modes for any m can appear, although only the $m=0$, 1, or 2 modes are primary bifurcation points in our investigations. Since the diffusion coefficients in the Gray–Scott model cannot be related to the experiments, we cannot predict which m will actually appear in the experiments.

Earlier investigators also interested in rotating waves in circularly symmetric geometries include [Auchmuty, 1979, 1984] and [Erneux and Herschkowitz-Kaufman, 1977, 1979a, 1979b], who both considered the Brusselator model on a two-dimensional disk. This model is nice to work with because it has a trivial solution and only two

chemical species, so analytical calculations are feasible. Unfortunately, as we will see below, for Hopf bifurcation in a model with two species the primary bifurcation is always to invariant periodic solutions, and bringing together Hopf points corresponding to different modes is impossible for nonzero diffusion coefficients. Thus local analysis cannot be used to find stable periodic solutions that have broken the $O(2)$ symmetry. [Erneaux and Herschkowitz-Kaufman, 1979a, 1979b] use numerical simulation in addition to local bifurcation theory and find that both standing and rotating waves can be stable. In our analysis these states can be found by secondary bifurcation.

3. Hopf bifurcation with $O(2)$ symmetry and mode interactions. In this section we briefly summarize concepts concerning Hopf bifurcation with $O(2)$ symmetry and the $O(2)$ Hopf–Hopf mode interactions. We give normal forms and describe the solutions that appear for each bifurcation, but we do not present details. This material is taken, for the most part, from [Golubitsky, Stewart, and Schaeffer, 1988] but we refer readers also to [Golubitsky and Roberts, 1987] and [Chossat, Golubitsky, and Keyfitz, 1986] for further details.

We first consider symmetry-breaking Hopf bifurcation with $O(2)$ symmetry. In our application this occurs when there are (nonzero) purely imaginary eigenvalues for some fixed positive value of m. Because the eigenvalues are reproduced for $-m$, the critical or center subspace is generically four-dimensional. As for Hopf bifurcation without symmetry, it is convenient to use complex coordinates, so we identify the four-dimensional space with $(z_1, z_2) \in C^2$. We will show in the Appendix how these coordinates are chosen so that they inherit the $O(2)$ action given by

$$\psi(z_1, z_2) = (e^{i\psi} z_1, e^{-i\psi} z_2), \qquad \kappa(z_1, z_2) = (z_2, z_1), \tag{3.1}$$

where ψ is the rotation and κ is the reflection. These coordinates were used by [van Gils and Mallet-Paret, 1984]. Because a Hopf bifurcation produces solutions periodic in time, there is an additional phase-shift symmetry [Golubitsky and Stewart, 1985], [Golubitsky, Stewart, and Schaeffer, 1988], that of the circle S^1, which acts by

$$\theta(z_1, z_2) = (e^{i\theta} z_1, e^{i\theta} z_2). \tag{3.2}$$

Details from the group theoretical standpoint of how this phase-shift symmetry arises are in the two previous references, but their result is that the normal form can be chosen to commute with the group $O(2) \times S^1$. This same result appears in the formal characterizations of normal forms of [Cushman and Sanders, 1986] and [Elphick et al., 1987]. Given the actions of $O(2)$ and S^1 above, it can be shown that a normal form for Hopf bifurcation with $O(2)$ symmetry can be represented up to any finite order by

$$\begin{pmatrix} \dot{z}_1 \\ \dot{z}_2 \end{pmatrix} = (p_1 + iq_1) \begin{pmatrix} z_1 \\ z_2 \end{pmatrix} + (r_1 + is_1)\delta \begin{pmatrix} z_1 \\ -z_2 \end{pmatrix}, \tag{3.3}$$

where $\delta = |z_2|^2 - |z_1|^2$ and the quantities p_1, q_1, r_1, and s_1 are real functions of $N = |z_1|^2 + |z_2|^2$, $\Delta = \delta^2$, the bifurcation parameter λ, and (in the case of degeneracies) other real parameters. Generically, there are two types of solutions to (3.3) near the origin: standing waves and rotating waves. In applications, it is important to note that the rotating waves appear in pairs that travel in opposite directions, but according to the theory they are identified as being essentially indistinguishable, since one is related to the other by the reflection κ, and thus behave identically. An important feature is that (3.3) can be separated into phase and amplitude equations and the resulting amplitude equations can be analyzed using singularity theory to obtain relatively complete

information on degenerate Hopf bifurcation up to codimension two [Golubitsky and Roberts, 1987].

As we said above, symmetry-breaking Hopf bifurcation occurs in our application when there are purely imaginary eigenvalues for some positive value of m. In the normal form (3.3) no trace of m remains and this deserves some explanation. Details are in [Golubitsky, Stewart, and Schaeffer, 1988] but the idea is that we factor out a cyclic kernel to obtain the standard action. This factoring out adds to the elegance of the theory but conceals the fact that the value of m is crucial to visualizing the appearance of the bifurcating solutions in the application. In the case of rotating waves on a circle, the value of m determines the number of peaks or wavefronts that appear.

The linear degeneracies that are of the most interest in this study are what we term Hopf–Hopf mode interactions, that is, bifurcation points where there are purely imaginary eigenvalues for more than one value of m simultaneously. We saw above that for equal diffusion coefficients this cannot happen and, furthermore, that the various modes (if they appear at all) appear in a very ordered fashion. Thus when we vary the diffusion coefficients away from equality, we would expect to see interactions between neighboring modes first. This turns out to be what we find for this model. Since the $m=0$ mode is the primary bifurcation for equal diffusion coefficients, we will focus on the $m=0$, $m=1$ Hopf–Hopf mode interaction, but we will also encounter the $m=0$, $m=2$ and $m=1$, $m=2$ interactions.

A general principle of local bifurcation theory is that it can be used to find stable bifurcating solutions only from the primary bifurcation. A step away from this limitation is the study of mode interactions, that is, situations where by varying one additional parameter we can get the bifurcation points for distinct modes to pass through each other. In such a situation each mode is the primary bifurcation for some parameter values and so can be expected to produce stable branches. A well-known result is that mode interactions can produce secondary or even tertiary bifurcations, which complicate the dynamics substantially. Studying these interactions via normal forms permits us to predict considerably more about the behavior of the system than can be determined from studying either mode alone. In our application, we are primarily interested in two types of Hopf–Hopf mode interactions.

The first type is the interaction of an invariant Hopf ($m=0$) and a symmetry-breaking Hopf ($m\neq 0$). The center manifold for this singularity is six-dimensional, and again complex coordinates (z_0, z_1, z_2) are the most convenient. We refer the reader to [Chossat, Golubitsky, and Keyfitz, 1986] for details. They show that if the two frequencies are incommensurate, the normal form commutes with the action of $O(2)\times T^2$ generated by

$$\begin{aligned}
&\psi(z_0, z_1, z_2) = (z_0, e^{i\psi}z_1, e^{-i\psi}z_2), \quad \psi\in SO(2)\subset O(2),\\
&\kappa(z_0, z_1, z_2) = (z_0, z_2, z_1),\\
&(\theta, \varphi)(z_0, z_1, z_2) = (e^{i\theta}z_0, e^{i\varphi}z_1, e^{i\varphi}z_2), \quad (\theta, \varphi)\in T^2.
\end{aligned} \tag{3.4}$$

Note that again it is the standard action of $O(2)$ that appears in (3.4), but the same warning for interpreting the results applies. The normal form for this singularity can be written as

$$\begin{pmatrix}\dot z_0\\ \dot z_1\\ \dot z_2\end{pmatrix} = (p_0+iq_0)\begin{pmatrix}z_0\\0\\0\end{pmatrix} + (p_1+iq_1)\begin{pmatrix}0\\z_1\\z_2\end{pmatrix} + (p_2+iq_2)\delta\begin{pmatrix}0\\z_1\\-z_2\end{pmatrix}, \tag{3.5}$$

where p_0, q_0, p_1, q_1, p_2, q_2 are functions of $\rho=|z_0|^2$, $N=|z_1|^2+|z_2|^2$, and $\Delta=\delta^2$, where

$\delta = |z_2|^2 - |z_1|^2$. Remarkably, (3.5) can be separated into phase and amplitude equations, which simplifies the analysis considerably. In fact, it should be possible to use singularity theory methods like those of [Golubitsky and Roberts, 1987] to classify the solutions to the amplitude in the case of degenerate six-dimensional Hopf–Hopf mode interactions, but this has not been done yet. What has been done [Chossat, Golubitsky, and Keyfitz, 1986] is to classify the solution types that appear at such a mode interaction and derive conditions that determine their stability. Luckily, it turns out that cubic terms in the normal form are sufficient in the nondegenerate case with which we will mainly be concerned. There are five basic types of solutions that generically appear at such a singularity. The first three are the primary branches that appear at the two individual Hopf points: an $O(2)$ invariant periodic solution originating at the invariant Hopf point, and standing waves and rotating waves associated with the $O(2)$ symmetry-breaking Hopf point. The two remaining types of solutions appear as secondary branches and are quasi-periodic, two-frequency motions that can be described as mixed modes that combine the invariant periodic solution with either the standing or rotating waves. These secondary branches appear simultaneously when they bifurcate from the invariant periodic solution, but individually when they bifurcate from the standing or rotating wave pure modes. Table 3.1 lists these five branches and identifies each with a number that will be used to identify the branch in § 5.

TABLE 3.1
Identification of branches for six-dimensional Hopf–Hopf interaction.

Branch	Identification
1	invariant periodic
2	rotating wave
3	standing wave
4	two frequency
6	two frequency

For our purposes, we need only consider the cubic order truncation of the amplitude equations

$$\begin{aligned} \dot{r}_0 &= r_0(p_{0,\lambda}\lambda + p_{0,\beta}\beta + p_{00}r_0^2 + p_{01}(r_1^2 + r_2^2)), \\ \dot{r}_1 &= r_1(p_{1,\lambda}\lambda + p_{1,\beta}\beta + p_{10}r_0^2 + p_{11}r_1^2 + p_{12}r_2^2), \\ \dot{r}_2 &= r_2(p_{1,\lambda}\lambda + p_{1,\beta}\beta + p_{10}r_0^2 + p_{12}r_1^2 + p_{11}r_2^2), \end{aligned} \tag{3.6}$$

which is obtained by truncating (3.5) at cubic order, writing $z_j = r_j e^{i\phi_j}$, and separating real and imaginary parts. Note that symmetry requires certain terms to equal; this is reflected in (3.6). This is not quite the same as the equations that are used in [Chossat, Golubitsky, and Keyfitz, 1986], but if $p_{0,\lambda} \neq 0$, $p_{1,\lambda} \neq 0$, and $p_{0,\lambda}p_{1,\beta} - p_{1,\lambda}p_{0,\beta} \neq 0$, (3.6) can be reduced to the case they consider by defining new bifurcation and unfolding parameters that are appropriate linear scalings and combinations of λ and β. If this can be done and ten additional nondegeneracy conditions involving the coefficients in (3.6) are satisfied, then the results of [Chossat, Golubitsky, and Keyfitz, 1986] allow us to determine the stabilities of the primary branches from each of the Hopf points and also locate and determine stability of branches originating from the secondary bifurcations. For the present study, it was found convenient to repeat the stability calculations without making a preliminary change of λ, β coordinates. The results are

TABLE 3.2
Branching equations and stabilities for six-dimensional Hopf-Hopf interaction.

Branch	Equation of branch	Eigenvalues on branch	Bifurcation point	Conditions for (<0): Supercritical bifurcation	Conditions for (<0): Stability at bifurcation point	Secondary bifurcation occurs at	Condition for secondary bifurcation (<0)
1	$\lambda = -\dfrac{p_{0,\beta}\beta + \varepsilon_{11} r_0^2}{p_{0,\lambda}}$	ε_{11} $\varepsilon_{\lambda\beta}\beta + \varepsilon_{21} r_0^2$	$\lambda = -\dfrac{p_{0,\beta}}{p_{0,\lambda}}\beta$	ε_{11}	ε_{11}, $\varepsilon_{\lambda\beta}\beta$	$\lambda_1 = -\dfrac{\eta_1}{\varepsilon_{31}}\beta$	$\dfrac{\varepsilon_{\lambda\beta}}{\varepsilon_{21}}\beta$ (1)
2	$\lambda = -\dfrac{p_{1,\beta}\beta + \varepsilon_{12} r_1^2}{p_{1,\lambda}}$	ε_{12}, ε_{22} $-\kappa\varepsilon_{\lambda\beta}\beta + \varepsilon_{32} r_1^2$	$\lambda = -\dfrac{p_{1,\beta}}{p_{1,\lambda}}\beta$	ε_{12}	ε_{12}, ε_{22} $-\kappa\varepsilon_{\lambda\beta}\beta$	$\lambda_2 = -\dfrac{\eta_2}{\varepsilon_{32}}\beta$	$-\dfrac{\varepsilon_{\lambda\beta}}{\varepsilon_{32}}\kappa\beta$ (2)
3	$\lambda = -\dfrac{p_{1,\beta}\beta + \varepsilon_{13} r_1^2}{p_{1,\lambda}}$	ε_{13}, ε_{23} $-\kappa\varepsilon_{\lambda\beta}\beta + \varepsilon_{33} r_1^2$	$\lambda = -\dfrac{p_{1,\beta}}{p_{1,\lambda}}\beta$	ε_{13}	ε_{13}, ε_{23}, $-\kappa\varepsilon_{\lambda\beta}\beta$	$\lambda_3 = -\dfrac{\eta_3}{\varepsilon_{33}}\beta$	$-\dfrac{\varepsilon_{\lambda\beta}}{\varepsilon_{33}}\kappa\beta$ (3)
4	$\lambda = -\dfrac{p_{0,\beta}\beta + \varepsilon_{11} r_0^2 + p_{01} r_1^2}{p_{0,\lambda}}$	ε_{22}	λ_1	$-\dfrac{p_{0,\lambda}\varepsilon_{21}}{\det 4}$	ε_{11}, ε_{22}, $-\det 4$	λ_4	(1), $-\det 4$, and $\xi_1\varepsilon_{31}\varepsilon_{11}$* or $\varepsilon_{11}\varepsilon_{12}$
	$\varepsilon_{\lambda\beta}\beta = \kappa\varepsilon_{32} r_1^2 - \varepsilon_{21} r_0^2$	$\det 4 = \varepsilon_{11}\varepsilon_{12} - p_{01}p_{10}$ $\text{trace} = \varepsilon_{11} r_0^2 + \varepsilon_{12} r_1^2$	λ_2	$-\dfrac{p_{1,\lambda}\varepsilon_{32}}{\det 4}$	ε_{12}, ε_{22}, $-\det 4$	λ_4	(2), $-\det 4$, and $\xi_1\kappa\varepsilon_{32}\varepsilon_{12}$* or $\varepsilon_{11}\varepsilon_{12}$
6	$\lambda = -\dfrac{p_{0,\beta}\beta + \varepsilon_{11} r_0^2 + 2p_{01} r_1^2}{p_{0,\lambda}}$	ε_{23}	λ_1	$-\dfrac{p_{0,\lambda}\varepsilon_{31}}{\det 6}$	ε_{23}, ε_{11} $-\det 6$	λ_6	(2), $-\det 6$, and $\xi_2\kappa\varepsilon_{32}\varepsilon_{12}$* or $\varepsilon_{11}\varepsilon_{13}$
	$\beta = \dfrac{\kappa\varepsilon_{33} r_1^2 - \varepsilon_{21} r_0^2}{\varepsilon_{\lambda\beta}}$	$\det 6 = \varepsilon_{11}\varepsilon_{13} - 2p_{10}p_{01}$ $\text{trace} = \varepsilon_{11} r_0^2 + \varepsilon_{13} r_1^2$	λ_3	$-\dfrac{p_{1,\lambda}\varepsilon_{33}}{\det 6}$	ε_{23}, ε_{13} $-\det 6$	λ_6	(3), $-\det 6$, and $\xi_2\kappa\varepsilon_{33}\varepsilon_{13}$* or $\varepsilon_{11}\varepsilon_{13}$

* Unbounded secondary branches only.

summarized in Table 3.2 (based on Table 4.5 in [Chossat, Golubitsky, and Keyfitz, 1986]), with the definitions needed to evaluate the quantities appearing in Table 3.2 given in Table 3.3. The reader should note that Table 3.2 is considerably more useful for applications. The ε_{ij} matrix appearing in the tables is similar to one defined in [Melbourne, Chossat, and Golubitsky, 1989], which turns out to be very useful in determining the stabilities of the three primary branches. For example, if the entries in the jth column are all negative, then branch j will be stable when it originates from the primary bifurcation point and will become stable via secondary bifurcations when the other mode bifurcates first.

TABLE 3.3
Definitions of quantities in Table 3.2.

$$\varepsilon_{11} = p_{00} \qquad \varepsilon_{21} = (p_{0,\lambda}p_{10} - p_{1,\lambda}p_{00})/p_{0,\lambda}$$
$$\varepsilon_{12} = p_{11} \qquad \varepsilon_{22} = p_{12} - p_{11}$$
$$\varepsilon_{13} = p_{11} + p_{12} \qquad \varepsilon_{23} = p_{11} - p_{12}$$
$$\varepsilon_{31} = (p_{0,\lambda}p_{10} - p_{1,\lambda}p_{00})/p_{0,\lambda}$$
$$\varepsilon_{32} = (p_{1,\lambda}p_{01} - p_{0,\lambda}p_{11})/p_{1,\lambda}$$
$$\varepsilon_{33} = [2p_{1,\lambda}p_{01} - p_{0,\lambda}(p_{11} + p_{12})]/p_{1,\lambda}$$
$$\kappa = \frac{P_{1,\lambda}}{p_{0,\lambda}} \qquad \varepsilon_{\lambda\beta} = \frac{p_{0,\lambda}p_{1,\beta} - p_{1,\lambda}p_{0,\beta}}{p_{0,\lambda}}$$
$$\eta_1 = \frac{p_{10}p_{0,\beta} - p_{00}p_{1,\beta}}{p_{0,\lambda}} \qquad \eta_2 = \frac{p_{01}p_{1,\beta} - p_{11}p_{0,\beta}}{p_{1,\lambda}} \qquad \eta_3 = \frac{2p_{01}p_{1,\beta} - (p_{11} + p_{12})p_{0,\beta}}{p_{1,\lambda}}$$
$$\xi_1 = \varepsilon_{12}\varepsilon_{21} + \kappa\varepsilon_{11}\varepsilon_{32} \qquad \xi_2 = \varepsilon_{13}\varepsilon_{31} + \kappa\varepsilon_{11}\varepsilon_{33}$$
$$\lambda_4 = -(\varepsilon_{12}\eta_1 + \kappa\varepsilon_{11}\eta_2)/\xi_1 \qquad \lambda_6 = -(\varepsilon_{13}\eta_1 + \kappa\varepsilon_{11}\eta_3)/\xi_2$$

It can also be shown that seven of the ten nondegeneracy conditions of [Chossat, Golubitsky, and Keyfitz, 1986] are equivalent to requiring no nonzero entries in the ε_{ij} matrix (the careful reader will have already noted that $\varepsilon_{21} = \varepsilon_{31}$ and $\varepsilon_{22} = -\varepsilon_{23}$, so there are only seven independent entries). Their remaining three conditions are provided by requiring nonzero values for p_{12}, det 4, and det 6. Note that since (3.6) is more general than the normal form considered in [Chossat, Golubitsky, and Keyfitz, 1986] we additionally require nonzero values for $p_{0,\lambda}$, $p_{1,\lambda}$ and $p_{0,\lambda}p_{1,\beta} - p_{1,\lambda}p_{0,\beta}$ $(= p_{0,\lambda}\varepsilon_{\lambda\beta})$, bringing the total number of nondegeneracy conditions to 13. If these conditions are satisfied, then the direction of branching and stability of each of the five primary and secondary branches is determined by the cubic order truncated normal form (3.6). In addition, any secondary bifurcation points that appear for a fixed value of $\beta \neq 0$ will do so at distinct values of λ. If any one of them is not satisfied, then further analysis must be done.

The final singularity of interest is the interaction of two $O(2)$ symmetry-breaking Hopf bifurcations, which has an eight-dimensional center manifold. Complex coordinates $(z_1, z_2, z_3, z_4) \in C^2 \oplus C^2$ are again the most convenient. When the frequencies are nonresonant, the relevant symmetry group is again $O(2) \times T^2$ as it was for the six-dimensional interaction, but the action is more complicated since $O(2)$ does not act trivially on any of the coordinates, as it did on z_0 in the previous case. Using the same notation as above, the relevant action is generated by

$$\psi(z_1, z_2, z_3, z_4) = (e^{ik\psi}z_1, e^{-ik\psi}z_2, e^{in\psi}z_3, e^{-in\psi}z_4), \quad \psi \in SO(2) \subset O(2),$$
$$\kappa(z_1, z_2, z_3, z_4) = (z_2, z_1, z_4, z_3), \tag{3.7}$$
$$(\theta, \varphi)(z_1, z_2, z_3, z_4) = (e^{i\theta}z_1, e^{i\theta}z_2, e^{i\varphi}z_3, e^{i\varphi}z_4), \quad (\theta, \varphi) \in T^2.$$

The integers k and n, $k<n$, that appear in (3.7) are the values of m to which the two Hopf points correspond. In our application we will be interested in the case where $k=1$ and $n=2$. More generally, the values of k and n are obtained by removing common factors between the two values of m and factoring out by a cyclic kernel, but we do not need this generality. We do note, however, that in the general case it is not possible to assume that $O(2)$ acts via its standard representation on (z_1, z_2), even though this turns out to be possible for the case we consider here.

The normal form for the eight-dimensional Hopf–Hopf interaction is developed in detail in [Chossat, Golubitsky, and Keyfitz, 1986]. We merely reproduce the final result:

$$\begin{aligned}
\dot{z}_1 &= (p_1+iq_1)z_1+(r_1+is_1)\bar{z}_1^{n-1}z_2^n(z_3\bar{z}_4)^k,\\
\dot{z}_2 &= (p_2+iq_2)z_2+(r_2+is_2)z_1^n\bar{z}_2^{n-1}(\bar{z}_3z_4)^k,\\
\dot{z}_3 &= (p_3+iq_3)z_3+(r_3+is_3)(z_1\bar{z}_2)^n\bar{z}_3^{k-1}z_4^k,\\
\dot{z}_4 &= (p_4+iq_4)z_4+(r_4+is_4)(\bar{z}_1z_2)^nz_3^k\bar{z}_4^{k-1},
\end{aligned} \tag{3.8}$$

where the real functions p_j, q_j, r_j, s_j, $j=1,4$ depend on $\rho_i=|z_i|^2$, $i=1,4$ and the real and imaginary parts of $\alpha=(z_1\bar{z}_2)^n(\bar{z}_3z_4)^k$. In addition, the reflection κ imposes relations between the first and second and third and fourth components of the vector field, which are easiest to describe as follows. Suppose that we represent (3.8) by $\dot{z}_j=F_j(z_1, z_2, z_3, z_4)$, $j=1,4$. Then the restrictions that are placed on the vector field by κ are

$$\begin{aligned}
F_2(z_1, z_2, z_3, z_4) &= F_1(\kappa(z_1, z_2, z_3, z_4)) = F_1(z_2, z_1, z_4, z_3),\\
F_4(z_1, z_2, z_3, z_4) &= F_3(\kappa(z_1, z_2, z_3, z_4)) = F_3(z_2, z_1, z_4, z_3).
\end{aligned} \tag{3.9}$$

A major difference from the six-dimensional normal form is that the eight-dimensional normal form cannot be separated into phase and amplitude equations, so the analysis is correspondingly more difficult. Also, adding to the complication in the eight-dimensional case are the four primary branches and the eight types of two- and three-frequency secondary branches that appear in this interaction. In [Chossat, Golubitsky, and Keyfitz, 1986] the branches that can appear in this interaction are classified, and conditions that allow the direction of bifurcation and stability of each branch to be determined are derived. Fortunately, in this study we are concentrating on the rotating waves, and it turns out that their branching and stability are determined at third order, including the behavior of the secondary branches that generically appear on the two branches of rotating waves. Furthermore, the normal form truncated at cubic order does separate into phase and amplitude equations so we can proceed as for the six-dimensional interaction and write our truncated normal form amplitude equations as

$$\begin{aligned}
\dot{r}_1 &= r_1(p_{1,\lambda}\lambda+p_{1,\beta}\beta+p_{11}r_1^2+p_{12}r_2^2+p_{13}r_3^2+p_{14}r_4^2),\\
\dot{r}_2 &= r_2(p_{1,\lambda}\lambda+p_{1,\beta}\beta+p_{12}r_1^2+p_{11}r_2^2+p_{14}r_3^2+p_{13}r_4^2),\\
\dot{r}_3 &= r_3(p_{3,\lambda}\lambda+p_{3,\beta}\beta+p_{31}r_1^2+p_{32}r_2^2+p_{33}r_3^2+p_{34}r_4^2),\\
\dot{r}_4 &= r_4(p_{3,\lambda}\lambda+p_{3,\beta}\beta+p_{32}r_1^2+p_{31}r_2^2+p_{34}r_3^2+p_{33}r_4^2).
\end{aligned} \tag{3.10}$$

Again, note the terms forced to be equal by symmetry. Following the classification of solutions in [Chossat, Golubitsky, and Keyfitz, 1986], we can construct Table 3.4, which provides identifying numbers for the four primary branches and the two secon-

TABLE 3.4
Branch identification for eight-dimensional Hopf–Hopf interaction.

Branch	Identification
1	k-rotating wave
2	k-standing wave
3	n-standing wave
4	n-rotating wave
7	two frequency
8	two frequency

dary branches, which generically bifurcate from the rotating waves. We also construct Table 3.5, which gives the branching equations and eigenvalues for these six branches. Table 3.6 provides the definitions of the quantities in Table 3.5. Using the results in the three tables, in § 5 we will be able to determine local bifurcation diagrams for the eight-dimensional Hopf–Hopf interaction, but only in a limited sense since we will ignore the branches of standing waves and their secondary bifurcations. It will turn out, however, that for the parameter values we have chosen, the rotating waves are the only stable solutions and the deficiency in our analysis will not be important.

It turns out that even for our limited analysis of the truncated normal form (3.10) there are 23 nondegeneracy conditions, i.e., these conditions must be satisfied for the direction of branching and stability of the four primary branches and two secondary branches we are considering to be determined at third order. Twelve of these conditions come from requiring that all of the ε_{ij} matrix entries be nonzero, $p_{1,\lambda} \neq 0$ and $p_{3,\lambda} \neq 0$ follow from requiring strict eigenvalue crossing, and the remaining nine conditions are derived by requiring distinct values of λ (for $\beta \neq 0$) for all of the primary and secondary bifurcation points. These conditions are summarized in Table 3.7.

4. Invariant steady-states and linear stability. In this section we want to establish in detail the structure and linear stability of the $O(2)$-invariant solutions. Our main interest continues to be symmetry-breaking Hopf bifurcations, but the preliminary material in this section lays the foundation for our later results. The techniques are singularity theory [Golubitsky and Schaeffer, 1985] and the global extensions due to [Balakotaiah and Luss, 1984] to determine the local structure of the invariant solutions and straightforward manipulation of the characteristic equation to determine stability.

The invariant steady-states are obtained by removing the diffusion terms from (2.5) and studying the steady-states of the resulting set of ordinary differential equations

$$\begin{aligned} \dot{x} &= -\beta x y^2 + \alpha_1 y^3 + \lambda(1-x), \\ \dot{y} &= \beta x y^2 - \alpha_1 y^3 - y + \alpha_3 z + \lambda(\gamma_2 - y), \\ \dot{z} &= y - \alpha_3 z + \lambda(\gamma_3 - z). \end{aligned} \tag{4.1}$$

These equations will be referred to below as the CSTR equations, since they describe the behavior of the Gray–Scott model in a continuous stirred tank reactor. As described in [Balakotaiah, 1987] the steady-states of (4.1) can be found from a single equation, cubic in y, that is obtained by setting the right-hand side of (4.1) to zero and eliminating the variables x and z. Furthermore, as shown in [Balakotaiah, 1987], the structure of the solutions of this cubic equation can be completely characterized via the singularity theory methods of [Golubitsky and Schaeffer, 1985] and the extensions in [Balakotaiah

TABLE 3.5
Branching equations and stabilities for eight-dimensional Hopf–Hopf interaction.

Branch	Equation of branch	Eigenvalues on branch	Bifurcation point	Conditions for (<0): Supercritical bifurcation	Conditions for (<0): Stability at bifurcation point	Secondary bifurcation occurs at	Condition for secondary bifurcation (<0)
1	$\lambda = -\dfrac{p_{1,\beta}\beta + p_{11}r_1^2}{p_{1,\lambda}}$	ε_{11}, ε_{21} $\varepsilon_{\lambda\beta}\beta + \varepsilon_{31}r_1^2$ $\varepsilon_{\lambda\beta}\beta + \varepsilon_{41}r_1^2$	$\lambda = -\dfrac{p_{1,\beta}}{p_{1,\lambda}}\beta$	ε_{11}	ε_{11}, ε_{21}, $\varepsilon_{\lambda\beta}\beta$	λ_{17} λ_{18}	$\dfrac{\varepsilon_{\lambda\beta}}{\varepsilon_{31}}\beta$ $\dfrac{\varepsilon_{\lambda\beta}}{\varepsilon_{41}}\beta$
2	$\lambda = -\dfrac{p_{1,\beta}\beta + \frac{1}{2}\varepsilon_{12}r_2^2}{p_{1,\lambda}}$	ε_{12}, ε_{22} $\varepsilon_{\lambda\beta}\beta + \varepsilon_{32}r_2^2$	$\lambda = -\dfrac{p_{1,\beta}}{p_{1,\lambda}}\beta$	ε_{12}	ε_{12}, ε_{22}, $\varepsilon_{\lambda\beta}\beta$	—	—
3	$\lambda = -\dfrac{p_{3,\beta}\beta + \frac{1}{2}\varepsilon_{13}r_3^2}{p_{3,\lambda}}$	ε_{13}, ε_{23} $-\kappa\varepsilon_{\lambda\beta}\beta + \varepsilon_{33}r_3^2$	$\lambda = -\dfrac{p_{3,\beta}}{p_{3,\lambda}}\beta$	ε_{13}	ε_{13}, ε_{23}, $-\kappa\varepsilon_{\lambda\beta}\beta$	—	—
4	$\lambda = -\dfrac{p_{3,\beta}\beta + p_{33}r_4^2}{p_{3,\lambda}}$	ε_{14}, ε_{24} $-\kappa\varepsilon_{\lambda\beta}\beta + \varepsilon_{34}r_4^2$ $-\kappa\varepsilon_{\lambda\beta}\beta + \varepsilon_{44}r_4^2$	$\lambda = -\dfrac{p_{3,\beta}}{p_{3,\lambda}}\beta$	ε_{14}	ε_{14}, ε_{24}, $-\kappa\varepsilon_{\lambda\beta}\beta$	λ_{47} λ_{48}	$-\dfrac{\varepsilon_{\lambda\beta}}{\varepsilon_{44}}\kappa\beta$ $-\dfrac{\varepsilon_{\lambda\beta}}{\varepsilon_{34}}\kappa\beta$
7	$\lambda = -\dfrac{p_{1,\beta}\beta + p_{11}r_1^2 + p_{13}r_2^2}{p_{1,\lambda}}$ $\beta = \dfrac{\kappa\varepsilon_{44}r_2^2 - \varepsilon_{31}r_1^2}{\varepsilon_{\lambda\beta}}$	$\varepsilon_{21}r_1^2 + (p_{14} - p_{13})r_2^2$ $(p_{32} - p_{31})r_1^2 + \varepsilon_{24}r_2^2$ $\det 7 = \varepsilon_{11}\varepsilon_{14} - 4p_{31}p_{13}$ $\text{trace} = \varepsilon_{11}r_1^2 + \varepsilon_{14}r_2^2$	λ_{17} λ_{47}	$-\dfrac{p_{1,\lambda}\varepsilon_{31}}{\det 7}$ $-\dfrac{p_{3,\lambda}\varepsilon_{44}}{\det 7}$	$\varepsilon_{11}, p_{32} - p_{31}$, $\varepsilon_{12}, -\det 7$ $\varepsilon_{14}, p_{14} - p_{13}$, $\varepsilon_{24}, -\det 7$	— —	— —
8	$\lambda = -\dfrac{p_{1,\beta} + \varepsilon_{11}r_1^2 + p_{14}r_2^2}{p_{1,\lambda}}$ $\beta = \dfrac{\kappa\varepsilon_{34}r_2^2 - \varepsilon_{41}r_1^2}{\varepsilon_{\lambda\beta}}$	$\varepsilon_{21}r_1^2 + (p_{13} - p_{14})r_2^2$ $(p_{31} - p_{32})r_1^2 + \varepsilon_{24}r_2^2$ $\text{trace} = \varepsilon_{11}r_1^2 + \varepsilon_{14}r_2^2$ $\det 8 = \varepsilon_{11}\varepsilon_{14} - 4p_{32}p_{14}$	λ_{18} λ_{48}	$-\dfrac{p_{1,\lambda}\varepsilon_{41}}{\det 8}$ $-\dfrac{p_{3,\lambda}\varepsilon_{34}}{\det 8}$	$\varepsilon_{21}, p_{31} - p_{32}$, $\varepsilon_{11}, -\det 8$ $\varepsilon_{24}, p_{13} - p_{14}$, $\varepsilon_{14}, -\det 8$	— —	— —

TABLE 3.6
Definitions of the quantities in Table 3.5.

$$\varepsilon_{11} = 2p_{11} \qquad \varepsilon_{21} = p_{12} - p_{11}$$
$$\varepsilon_{12} = 2(p_{11} + p_{12}) \qquad \varepsilon_{22} = 2(p_{11} - p_{12})$$
$$\varepsilon_{13} = 2(p_{33} + p_{34}) \qquad \varepsilon_{23} = 2(p_{33} - p_{34})$$
$$\varepsilon_{14} = 2p_{33} \qquad \varepsilon_{24} = p_{34} - p_{33}$$
$$\varepsilon_{31} = (p_{1,\lambda}p_{31} - p_{3,\lambda}p_{11})/p_{1,\lambda}$$
$$\varepsilon_{32} = [p_{1,\lambda}(p_{31} + p_{32}) - p_{3,\lambda}(p_{11} + p_{12})]/p_{1,\lambda}$$
$$\varepsilon_{33} = [p_{3,\lambda}(p_{13} + p_{14}) - p_{1,\lambda}(p_{33} + p_{34})]/p_{3,\lambda}$$
$$\varepsilon_{34} = (p_{3,\lambda}p_{14} - p_{1,\lambda}p_{33})/p_{3,\lambda}$$
$$\varepsilon_{41} = (p_{1,\lambda}p_{32} - p_{3,\lambda}p_{11})/p_{1,\lambda}$$
$$\varepsilon_{42} = [p_{1,\lambda}(p_{31} + p_{32}) - p_{3,\lambda}(p_{11} + p_{12})]/p_{1,\lambda}$$
$$\varepsilon_{43} = [p_{3,\lambda}(p_{13} + p_{14}) - p_{1,\lambda}(p_{33} + p_{34})]/p_{3,\lambda}$$
$$\varepsilon_{44} = (p_{3,\lambda}p_{13} - p_{1,\lambda}p_{33})/p_{3,\lambda}$$
$$\varepsilon_{\lambda\beta} = \frac{p_{1,\lambda}p_{3,\beta} - p_{1,\lambda}p_{3,\beta}}{p_{1,\lambda}} \qquad \kappa = \frac{p_{3,\lambda}}{p_{1,\lambda}}$$
$$\lambda_{17} = -\frac{p_{11}p_{3,\beta} - p_{31}p_{1,\beta}}{p_{11}p_{3,\lambda} - p_{31}p_{1,\lambda}} \qquad \lambda_{18} = -\frac{p_{32}p_{1,\beta} - p_{11}p_{3,\beta}}{p_{32}p_{1,\lambda} - p_{11}p_{3,\lambda}}$$
$$\lambda_{47} = -\frac{p_{13}p_{3,\beta} - p_{33}p_{1,\beta}}{p_{13}p_{3,\lambda} - p_{33}p_{1,\lambda}} \qquad \lambda_{48} = -\frac{p_{14}p_{3,\beta} - p_{33}p_{1,\beta}}{p_{14}p_{3,\lambda} - p_{33}p_{1,\lambda}}$$

TABLE 3.7
Nondegeneracy conditions for the eight-dimensional Hopf–Hopf interaction.

1-12	$\varepsilon_{ij} \neq 0 \quad i,j = 1,4$
13	$p_{1,\lambda} \neq 0$
14	$p_{3,\lambda} \neq 0$
15	$\varepsilon_{\lambda\beta} \neq 0$
16	$p_{11}p_{33} - p_{31}p_{13} \neq 0$
17	$p_{11}p_{33} - p_{32}p_{14} \neq 0$
18	$p_{11}p_{33} - p_{31}p_{14} \neq 0$
19	$p_{11}p_{33} - p_{32}p_{13} \neq 0$
20	$p_{13} \neq 0$
21	$p_{14} \neq 0$
22	$p_{31} \neq 0$
23	$p_{32} \neq 0$

and Luss, 1984]. For the present study we take λ as our distinguished bifurcation parameter, β and γ_2 as free parameters, and fix the values $\alpha_1 = 0.1$, $\alpha_3 = 0.002$, and $\gamma_3 = 0.4$. Given these values, the nonpersistence varieties and the corresponding steady-state bifurcation diagrams in the parameter regions of interest are shown in Fig. 5. Actually, the two steady-state limit points that occur in region 4 only enter tangentially into our analysis and can be ignored most of the time, so we can think of (4.1) as possessing a unique invariant steady-state. The numerical values on the axes correspond to sets B and C; an analogous plot for set A is qualitatively similar.

The next step is to study the linear stability of the invariant steady-states. The Gray–Scott model is simple enough so that this can be done using the characteristic

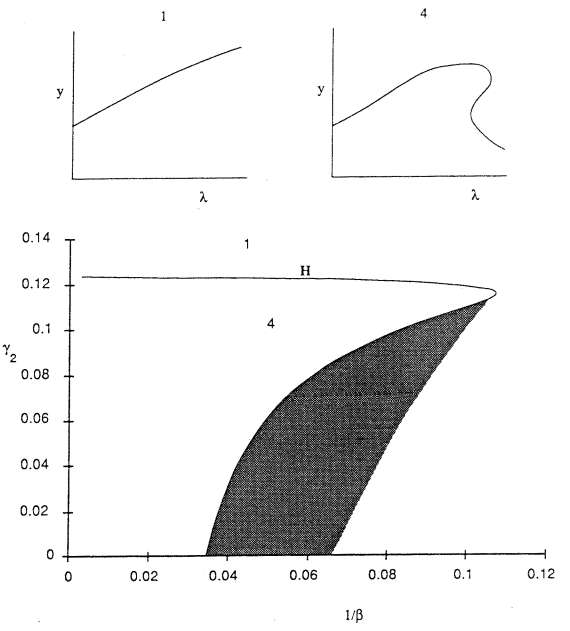

FIG 5. *Top: bifurcation diagrams for invariant steady-states. Numbers refer to open regions below. Bottom: nonpersistence variety* **H** *for invariant steady-states. Bifurcation variety* **B** *is the boundary of the shaded region.*

equation of the linearization of (2.5) about an invariant steady-state. At any invariant steady-state, the characteristic equation can be solved for the eigenvalues for each value of m. Clearly, we need only consider nonnegative values of m when determining linear stability, and, in fact, we will only need to consider a finite range for the values of m. However, it is not necessary to solve for all the eigenvalues if we are only interested in changes in stability. The idea is that we start our stability determination at some point where we know the eigenvalue configuration and then look for changes in stability as we move continuously along the invariant steady-state bifurcation diagram. Generically changes in stability occur via Hopf bifurcation or by a single real eigenvalue crossing through zero, and it is a simple matter to derive necessary conditions from the characteristic equation for each type of bifurcation point. These conditions are actually derived from the Routh-Hurwitz criterion [Levinson and Redheffer, 1970], which gives necessary and sufficient conditions for all of the eigenvalues to have negative real parts. This same criterion can be used to show that all eigenvalues have negative real part if λ is small but nonzero, giving us a starting point for determining linear stability. From the physical standpoint, having $\lambda = 0$ means that the system is closed and a continuum of uniform equilibrium states exists. Thus it comes as no surprise that close to equilibrium (i.e., small λ) the invariant steady-state is asymptotically stable.

To perform the linear stability analysis we must first choose values for the three diffusion coefficients. Since the Gray-Scott model is not intended to describe any particular physical system, there are no experimentally measured quantities to use as guides as there are for models more closely related to the B-Z system. We are guided, however, by our desire to see if the Gray-Scott model can exhibit behavior consistent with our interpretation of the experiments of [Noszticzius et al., 1987], that is, to choose the parameters so that the symmetry-breaking bifurcations are Hopf bifurcations that lead to stable rotating wave solutions. We would also like to see evidence that

different rotating modes can be simultaneously stable. With these goals in mind, we have chosen the three different sets of diffusion coefficient values shown in Table 4.1 below. For the sake of convenience we also include the values of the other fixed parameters for each set. Note that in set A the value of α_3 is changed to 0.01.

In general terms, we have found that if $D_1 \leqq D_2 < D_3$ then Hopf-Hopf mode interactions do occur and symmetry-breaking Hopf points can be primary bifurcation points. In addition, for this ordering of the diffusion coefficients, symmetry-breaking steady-state bifurcations are suppressed and do not interfere with our results. To be more precise, when there is a unique branch of invariant solutions (i.e., Fig. 5(a)), symmetry-breaking steady-state bifurcations do not occur. In parameter regions where there are multiple invariant steady-states, for any fixed value of λ there are either one or three such solutions. When there are three solutions we can speak of the middle branch and it is easy to see that this branch is unstable to perturbations with wave number $m = 0$. Symmetry-breaking steady-state bifurcation points do appear on these middle branches, but if the diffusion coefficients are ordered as above they stay on the middle branches and do not interact with our results. Furthermore, since the middle branch is unstable to perturbations with $m = 0$, any branch emerging from a symmetry-breaking steady-state bifurcation point on the middle branch of invariant solutions will itself be unstable near the bifurcation point.

The linear analysis for the three sets of parameters shown in Table 4.1 can be conveniently described by grouping sets B and C together, as the results are similar for this pair. Exactly what we mean by similar will be made clear below, but we note that we do not mean identical. Moreover, as we see in § 5, this similarity does not hold for the nonlinear analysis, and important differences between each of the three sets will emerge. In set A only the $m = 0$ and $m = 1$ Hopf points and their interaction are important. In sets B and C the $m = 2$ Hopf mode can also be a primary bifurcation point, and six-dimensional interactions between modes $m = 0$ and each of $m = 1$ and $m = 2$ are important, as well as the eight-dimensional $m = 1$, $m = 2$ interaction.

The linear analysis for set A is the simplest of the three sets and is a less complicated introduction to how we have chosen to present these results. Essentially, we will build on the results presented in Fig. 5 by adding curves to the parameter space plot, which represent important changes in the linear stability analysis. By important changes we generally mean changes in the number or relative positions of bifurcation points, e.g., degenerate Hopf bifurcations and mode interactions, *when these changes produce a change in the primary bifurcation point.* These additional curves, together with the steady-state nonpersistence curves we have already presented, divide the parameter plane into open regions. In each of these regions no important qualitative changes in the linear stability analysis occur, so we can represent each region with a single bifurcation diagram showing the relative locations of the Hopf bifurcation points. We will only give explicit results for the modes that actually become primary bifurcation points although we will usually give the largest value of m for which Hopf modes appear.

TABLE 4.1
Three parameter sets.

Set	D_1	D_2	D_3	α_1	α_3	γ_3
A	0.001	0.001	0.0013	0.1	0.01	0.4
B	0.001	0.0015	0.002	0.1	0.02	0.4
C	0.001	0.001	0.002	0.1	0.02	0.4

In Fig. 6 we have added two curves to those shown in Fig. 5 to describe the important features of the linear stability analysis for set A. These additional curves subdivide regions 1 and 4 into regions 1a–1c and 4a–4d. The new curves appearing in Fig. 6 can be divided into two classes. The first class describes stability changes for the CSTR version of the equations, that is, we restrict the analysis to the $m = 0$ subspace. These are shown in Fig. 6, along with the steady-state nonpersistence curves, as the thinner lines. These curves do not depend on the values of the diffusion coefficients and so are exactly the same for sets B and C of diffusion coefficients. We note that the CSTR linear stability results for set A are qualitatively similar to those of the other two sets. The important curves in this first class are labeled DH_0, representing a degenerate Hopf bifurcation in which a pair of $m = 0$ Hopf points appears and T-B represents the Takens–Bogdanov nilpotent double zero eigenvalue singularities. We make no serious attempt to analyze these latter singularities since we consider only Hopf bifurcations in this study, but we do note that they appear and that the DH_0 and six-dimensional Hopf–Hopf mode interaction curves terminate on the T-B curve. We note that the linear analysis follows the same pattern as shown in Fig. 3, with the invariant steady-state being stable (Fig. 3(a)) in regions 1a and 4a.

The second class of curves, shown as heavier lines in Fig. 6, represents changes in the linear stability analysis involving symmetry-breaking modes. Only two curves from this class appear in Fig. 6. The curve DH_1 represents a degenerate Hopf bifurcation in which a pair of $m = 1$ Hopf points appear between the two $m = 0$ Hopf points already present. On the curve labeled H-H a six-dimensional $m = 0$, $m = 1$ Hopf–Hopf mode interaction occurs and in the region labeled 4d in Fig. 6, the leftmost $m = 1$ Hopf point becomes a primary bifurcation point. For our analysis, this is the most important curve in the figure.

Because the parameter space plots (e.g., Fig. 6) are actually projections, curves may appear to cross when, in fact, they do not intersect. To avoid confusion, points of actual intersection are marked with dots in the parameter space plots. If two curves appear to cross but their intersection is not marked in this way, then the two degeneracies represented by the curves do not interact locally. For example, the curve DH_0 crosses the **H** curve twice in Fig. 6 but the degenerate Hopf bifurcation and the hysteresis

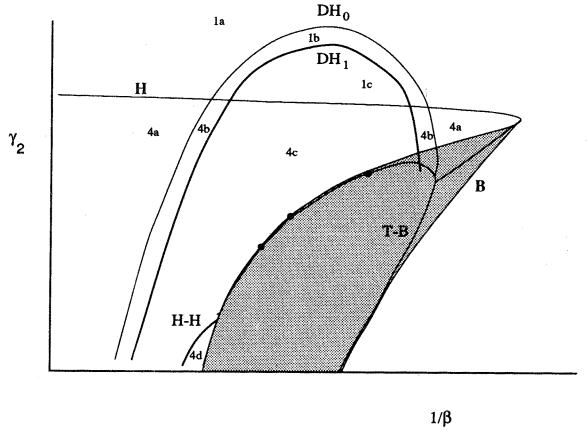

FIG. 6. *Additional curves DH_0 ($m = 0$ degenerate Hopf), DH_1 ($m = 1$ degenerate $O(2)$ Hopf), and H-H (six-dimensional $m = 0$, $m = 1$ Hopf–Hopf interaction) in parameter space, arising from linear stability analysis of set A.*

singularity occur at different values of λ. On the other hand, the **H** curve and the T-B curve have the two points of intersection marked in the figure. These are degenerate Takens-Bogdanov singularities for which one of the quadratic terms in the normal form vanishes. It is known that the dynamics near such a degeneracy can be quite complicated, but we will not address that here.

Figure 6 summarizes the most important aspects of the linear analysis for set *A*. Other Hopf modes (at least $m = 0$ to $m = 12$) appear and the size of region 4d is actually quite small. However only Hopf modes $m = 0$ and $m = 1$ can be primary bifurcation points for set *A*, so we neglect the other modes since our methods could not be used to obtain stable solutions involving them.

In the shaded region in Fig. 6, additional complications beyond the scope of this paper occur. These complications are caused by multiple invariant steady-states interacting with the Hopf bifurcations, producing the Takens-Bogdanov singularities mentioned above from the $m = 0$ Hopf points and invariant limit point, symmetry-breaking Hopf point interactions from the other Hopf modes. Further into this region, after the symmetry-breaking Hopf points pass through the invariant limit points, Takens-Bogdanov singularities with $O(2)$ symmetry [Dangelmayr and Knobloch, 1987] appear. We mention these singularities only in passing to illustrate the complications to be expected even in this rather simple model. In fact, the termination of the H-H curve on the T-B curve in Fig. 6 produces a singularity that has not yet been analyzed. Since it would contain both homoclinic behavior from the $m = 0$ Takens-Bogdanov singularity and periodic behavior from the symmetry-breaking Hopf bifurcation, homoclinic tangles and weakly chaotic behavior would almost surely be present.

In Fig. 7 we summarize the linear stability analysis for sets *B* and *C* of parameters. Two new curves appear that did not appear in Fig. 6. Along these curves, labeled H-H 0-2 and H-H 1-2, Hopf-Hopf interactions occur between the leftmost $m = 0$ and $m = 2$ Hopf points (H-H 0-2) and the leftmost $m = 1$ and $m = 2$ Hopf points (H-H 1-2). We call the reader's attention to the facts that the leftmost $m = 1$ Hopf point is still the primary bifurcation point on the H-H 0-2 curve and that the leftmost $m = 2$ Hopf point is a primary bifurcation point only in the small region labeled 4h. The three Hopf-Hopf interaction curves in Fig. 7 are drawn schematically. In fact, these curves lie very close to the invariant steady-state hysteresis curve **H** and could not be distinguished from it if the drawing was done to scale. Exact parameter values for some points on the Hopf-Hopf interaction curves will be presented in the next section. Tabulated results for all of the Hopf-Hopf interaction curves are available on request from the authors.

5. Nonlinear analysis and stable rotating waves. In this section we describe the results of our nonlinear analysis of invariant and symmetry-breaking Hopf bifurcations and Hopf-Hopf mode interactions. As the title of this section suggests, our focus is on using the local analysis to predict stable rotating wave solutions in the Gray-Scott model. Specifically, we use local analysis in this section to predict stable rotating wave solutions corresponding to modes $m = 1$ and $m = 2$. There are essentially two ways that we can do this. In the case where a symmetry-breaking Hopf point is a primary bifurcation point, a center manifold/normal form reduction to (3.3) truncated at some order, coupled with the results in [Golubitsky and Roberts, 1987] permits us, in principle, to predict local branching and stability, including the unfolding of degeneracies up to codimension two. In this paper we concentrate on the codimension-one degeneracies and present examples of each of the four types.

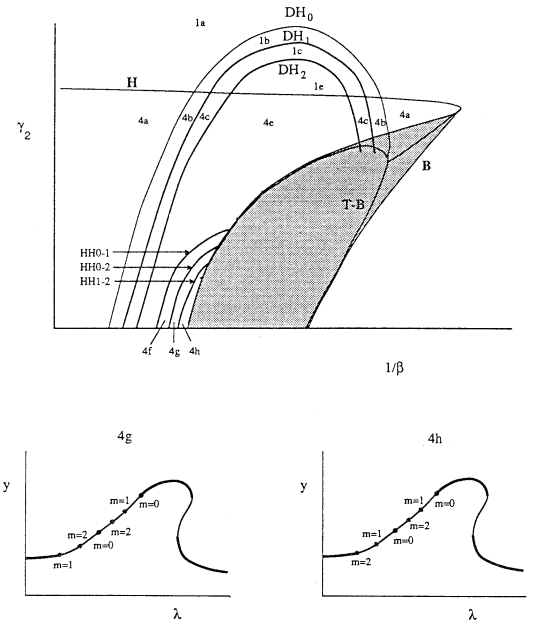

FIG. 7. *Top*: *Curves showing degenerate Hopf bifurcation* (DH_0, DH_1, DH_2) *and six- and eight-dimensional Hopf-Hopf interactions for sets B and C. Bottom*: *linear stability of invariant steady-states for sets B and C corresponding to open regions* 4g *and* 4h *above.*

On the other hand, we saw in § 4 that the region in parameter space where a symmetry-breaking Hopf bifurcation is primary becomes very small as we approach the physically realistic case of nearly equal diffusion coefficients. This brings analysis of the Hopf-Hopf mode interactions to the forefront because it allows us to predict stable symmetry-breaking periodic solutions originating from Hopf points that are not primary. Results in this section on the $m=0$, $m=1$ six-dimensional Hopf-Hopf interaction considerably extend the parameter space region of stable rotating waves for this model. A more complicated analysis involving the $m=1$, $m=2$ eight-dimensional and $m=0$, $m=2$ six-dimensional Hopf-Hopf interactions suggests that the $m=2$ rotating waves can be stable even when the $m=2$ Hopf point occurs to the right of both the $m=0$ and $m=1$ Hopf points and that the $m=1$ and $m=2$ rotating wave can be simultaneously stable. Both of these results are consistent with the experimental results of [Noszticzius et al., 1987]. The results for the $m=2$ rotating waves are weaker, as suggested by the wording of the previous sentence, than those for $m=1$; they do not prove stability in this situation but are merely consistent with it.

The discussion in this section is organized as follows. First, we describe results for the three parameter sets A-C on stable rotating waves for modes $m=1$ and $m=2$ produced via primary bifurcations. In doing so, we encounter examples of each of the four codimension -one degenerate $O(2)$ Hopf bifurcations of [Golubitsky and Roberts, 1987]. Tracking these degeneracies produces additional curves, which further subdivide the parameter space regions in Figs. 8 and 10. Computation of higher-order normal form coefficients on these curves of degenerate $O(2)$ Hopf bifurcation permits us to use the results of [Golubitsky and Roberts, 1987] to predict the existence and the position of limit points on the rotating wave (type III degeneracy) and standing wave (type II degeneracy) branches and the existence of secondary bifurcations to two-frequency solutions (type IV degeneracy).

Next, we consider the $m=0$, $m=1$ six-dimensional Hopf–Hopf interactions for each set of parameters and describe the parameter space regions where this analysis predicts stable $m=1$ rotating waves when the $m=0$ Hopf point is the primary bifurcation point. In general, we find that we can do so for sets B and C but not for set A, for which the $m=1$ standing waves are the stable solution. Degeneracies on the six-dimensional Hopf–Hopf interaction curves are considered in a limited way: we distinguish degeneracies due to the interaction of the codimension-one degenerate $O(2)$ Hopf curves described above with the Hopf–Hopf curve from those that arise purely in the interaction. Partial results can be obtained for the first class of degeneracies, and reasonable conjectures can be stated for the second class.

Finally, we describe the results for the $m=1$, $m=2$ eight-dimensional Hopf–Hopf interactions that occur in sets B and C. We do not discuss degeneracies in any detail, but we do identify a region in parameter space for set C where the $m=1$ and $m=2$ rotating waves are simultaneously stable.

5.1. Stable rotating waves via primary bifurcations. We recall (cf. [Golubitsky and Roberts, 1987]) that in a generic $O(2)$ Hopf bifurcation two families of periodic solutions emerge from a nondegenerate $O(2)$ symmetry-breaking Hopf point: a rotating family and a standing wave family. Moreover, neither branch can be stable unless both families bifurcate supercritically, in which case exactly one family is stable. The results in this section are obtained by computing the cubic order truncated normal form for the leftmost $m=1$ and $m=2$ Hopf points in the regions (if any) where they are primary bifurcation points and by using the results in [Golubitsky and Roberts, 1987] to determine the local diagrams. When codimension-one degeneracies are encountered, the curves of degenerate $O(2)$ Hopf bifurcation are also computed, since they divide the primary regions into subregions. In each subregion the local diagrams predicted by the cubic order truncation are qualitatively the same. By computing higher-order terms on the curves of codimension-one degenerate $O(2)$ Hopf bifurcation, we obtain more information on the diagrams for parameter values in a neighborhood of the curve, as well as detecting codimension-two degeneracies. We now describe our results for each of the three sets in turn.

5.1.1. Set *A*. The behavior of set A is quite different from that of sets B and C. One main difference is that the $m=1$ standing waves can be stable. As described in the previous section, the leftmost $m=1$ Hopf point is a primary bifurcation point in the small region labeled 4d. In Fig. 8 we show a schematic blow-up of this region and include the three codimension-one degenerate $O(2)$ Hopf bifurcation curves that pass through this region. We show the local diagrams for each of the four open subregions, as determined from the cubic order truncated normal form, as the upper row of bifurcation diagrams in Fig. 8. In the bottom row of bifurcation diagrams in the figure, we show results valid in a neighborhood of the degeneracy curves, obtained by computing the normal form up to fifth order.

The type IV degenerate $O(2)$ Hopf bifurcation is interesting because it produces a quasi-periodic secondary branch, which connects the rotating wave and standing wave families. A complete analysis of this degeneracy [Golubitsky and Roberts, 1987] requires seventh-order terms in the normal form, and these have not yet been computed. However, the stabilities of the rotating wave and standing wave branches and the parameter region where the secondary branch exists are all determined by the fifth-order terms. Thus in Fig. 8 we show that the secondary branch (labeled T) exists in subregion $4d_4$, that the rotating wave branch is destabilized, and that the standing wave branch

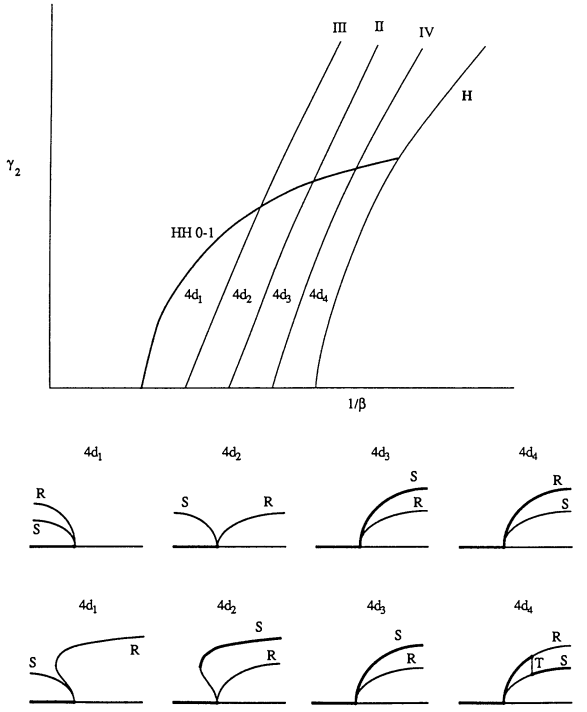

FIG. 8. *Results of nonlinear $O(2)$ Hopf bifurcation analysis of set A in the region where the leftmost $m=1$ Hopf point is a primary bifurcation point. The bottom row of bifurcation diagrams was produced by including fifth-order terms.*

is stabilized by the secondary bifurcations. Our lack of stability information for the T branch is reflected in the figure by drawing it as a vertical line.

5.1.2. Sets *B* and *C*. It is convenient to combine our description of these two sets. Recall that the parameter values of these two sets differ only in that $D_2=0.0015$ for set B, but $D_2=0.001$ for set C. As described in § 4, both sets have regions where the leftmost $m=1$ and $m=2$ Hopf points are primary bifurcation points. In Figs. 9 (set B) and 10 (set C) we show schematic drawings of these regions including the codimension-one degenerate $O(2)$ Hopf curves that divide the regions into subregions.

We remark that each codimension-one degenerate Hopf curve corresponds to either the leftmost $m=1$ or leftmost $m=2$ Hopf point. For example, the curve labeled III-1 signifies a type III codimension-one degenerate $O(2)$ Hopf bifurcation for the leftmost $m=1$ Hopf point. Strictly speaking, in a region where one of the two Hopf points is a primary bifurcation point, only the codimension-one degenerate $O(2)$ Hopf curves divide that region into subregions of qualitatively different bifurcation diagrams for the primary bifurcation point. For the $m=2$ Hopf points, we are unable to predict stable $m=2$ rotating waves for set B because the type III degenerate $O(2)$ Hopf curve never enters region 4h. For set C stable $m=2$ rotating waves exist in subregion $4h_1$ and in a neighborhood of the type III degenerate $O(2)$ Hopf curve in subregion $4h_2$.

The situation for the $m=1$ Hopf point is more complicated. Certain features are shared between the two sets, and we describe these first. For both sets B and C there are type II, III, and IV degenerate $O(2)$ Hopf curves appearing. The type IV curve

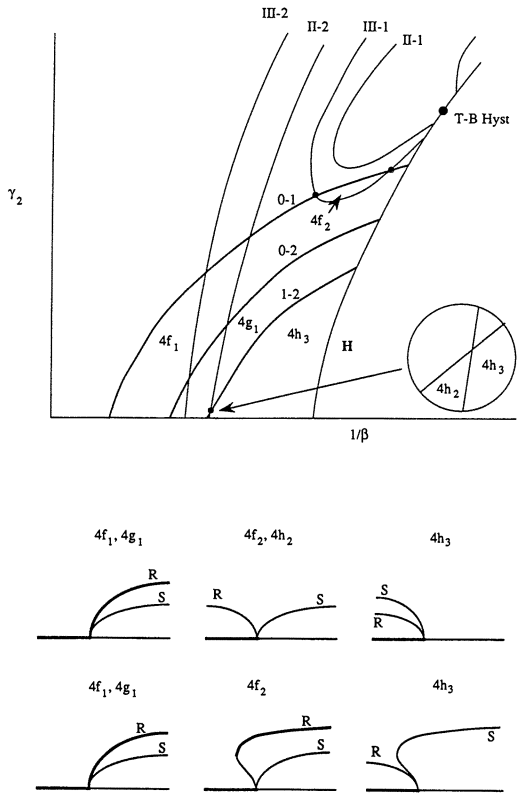

FIG. 9. *Results of $O(2)$ Hopf bifurcation analysis for set B, showing regions where the $m=1$ and $m=2$ Hopf points are primary bifurcation points.*

for set B lies entirely outside regions 4f and 4g and will not be part of our analysis. The type IV curve for the $m=1$ Hopf point in set C has a small part inside region 4f, but aside from noting the existence of potentially very interesting type IX and X [Golubitsky and Roberts, 1987] codimension-two degenerate $O(2)$ Hopf bifurcation points on the type IV curve, we will not discuss this curve in detail either.

The type II and III degenerate $O(2)$ Hopf curves for sets B and C are similar in shape and position relative to the hysteresis curve **H**. In fact, the actual positions of the two curves change little as D_2 is decreased. Recall from § 4 that decreasing the value of D_2 from 0.0015 to 0.001 moved the three Hopf–Hopf interaction curves to larger values of γ_2. Thus most of the more complicated structure for set C is because the Hopf–Hopf interaction curves moved so that they now have more intersections with the codimension-one degenerate $O(2)$ Hopf curves. There are certain differences, however, such as the two codimension-two degenerate Hopf singularities referred to above. Note also that the termination point of the $m=0$, $m=1$ six-dimensional Hopf–Hopf interaction curve on the curve of $m=0$ Takens–Bogdanov singularities (which is not shown in the figure, since it lies very close to the hysteresis curve) for set C is very close to the degenerate Takens–Bogdanov hysteresis singularity. We conjecture that this proximity is at least partially responsible for the complicated behavior of the $m=1$ Hopf point referred to above and the degeneracies we encounter when we describe the $m=0$, $m=1$ six-dimensional Hopf–Hopf interaction results below.

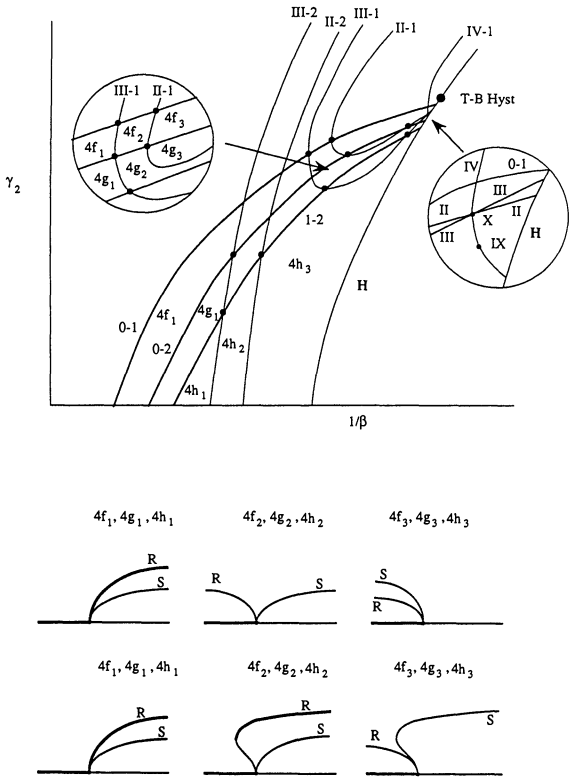

FIG 10. *Results of $O(2)$ Hopf bifurcation analysis for set C, showing regions where the $m = 1$ and $m = 2$ Hopf points are primary bifurcation points.*

5.2. Six-dimensional Hopf–Hopf mode interactions. In this section we report our computations and analysis of the cubic order truncated normal form on the curves of six-dimensional Hopf-Hopf interactions and use the results summarized in § 3 to predict the stability of symmetry-breaking periodic solutions originating at Hopf points that are not primary bifurcation points. In other words, we extend our results on stable symmetry-breaking periodic solutions outside the regions of § 5.1. A simple observation is that the symmetry-breaking periodic solution must be stable when it originates from a primary bifurcation point to restabilize via secondary bifurcation on the other side of the mode interaction curve. Thus the results of § 5.1 clearly define the regions where we can hope to obtain stable symmetry-breaking periodic solutions from bifurcation points that are not primary via mode interactions.

When we consider the six-dimensional Hopf-Hopf interactions for the three sets A-C of parameter values from this point of view, it turns out that there are only seven sets of local bifurcation diagrams that are important to our analysis, and these are shown in Fig. 11. Table 5.1 summarizes our six-dimensional Hopf-Hopf interaction results for the Gray-Scott model, providing values of β and γ_2 and local diagram identifications corresponding to those in Fig. 11. As a convention, we are using β to represent both a model parameter and an unfolding parameter in the normal form. The values of β in Table 5.1 are actual values of the model parameter, while in the local diagrams in Fig. 11, β represents a deviation of β from its value on the Hopf-Hopf interaction curve. Identifications in the table marked with an asterisk mean that the

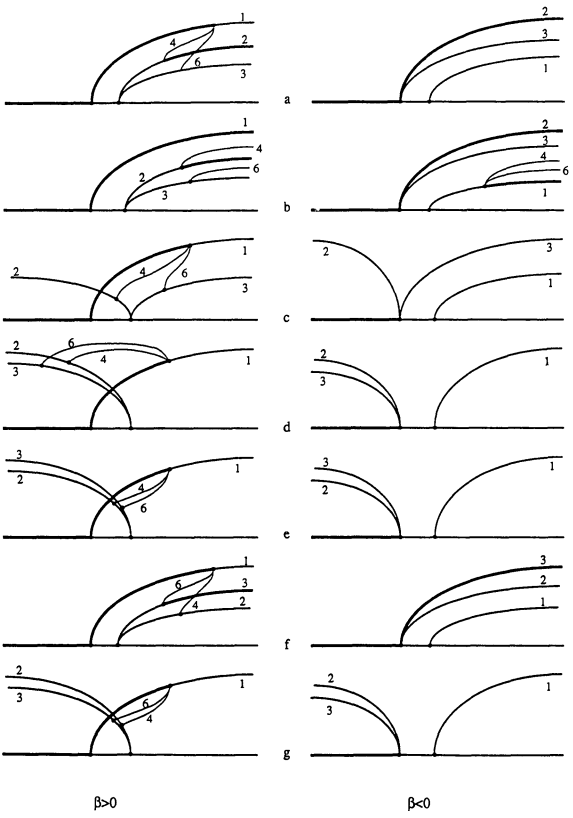

FIG. 11. *Local diagrams for the seven most important distinct six-dimensional Hopf-Hopf interactions found in the Gray-Scott model.*

diagram is not one of the seven found in Fig. 11 and also that several degeneracies occur nearby, so the results are not well represented by a single set of diagrams. The most interesting diagrams from a practical standpoint are *a*, *b*, and *f* since they predict stable symmetry-breaking branches. Coincidentally, the most common diagrams for the $m = 0$, $m = 1$ interactions, in terms of persistence over large parameter ranges are also *a*, *b*, and *f*. Thus the overall result is that the $m = 1$ rotating wave generally stabilizes via a secondary bifurcation for sets B and C of parameter values, and the $m = 1$ standing wave stabilizes for set A.

A change in the diagram designation in Table 5.1 means that at least one of the nondegeneracy conditions for the six-dimensional Hopf–Hopf interaction has been violated between the two entries. The nondegeneracy conditions fall into two general classes. The simplest class occurs when the direction of branching of one of the three primary branches changes. In a sense to be made more precise below, these types of degeneracies can be partially understood by considering higher-order terms for that particular branch, which simplifies the calculation considerably. More difficult to handle are degeneracies involving the secondary branches, requiring higher-order terms in the six-dimensional normal form and analysis that remains to be done. We will describe examples from each class in our discussion below. In general, for sets B and A the only degeneracies on the $m = 0$, $m = 1$ Hopf–Hopf interaction curve are of the simpler type arising from degenerate $O(2)$ Hopf bifurcations. For set C the second type of degeneracy occurs as well. In fact, for set C no less than seven degeneracies

TABLE 5.1
Six-dimensional Hopf–Hopf interactions for sets A–C. Letters a–g *refer to Fig.* 11.

Set *A*	β	4.87E+01	4.92E+01	4.97E+01	5.02E+01	5.07E+01	5.12E+01	5.17E+01	5.22E+01	5.27E+01	5.32E+01
	γ_2	2.26E−02	2.08E−02	1.90E−02	1.71E−02	1.52E−02	1.33E−02	1.14E−02	9.41E−03	7.44E−03	5.44E−03
0-1	Dia.	a	f	f	f	f	f	*	g	g	g
Set *B*	β	2.12E+01	2.20E+01	2.28E+01	2.36E+01	2.44E+01	2.52E+01	2.60E+01	2.68E+01	2.76E+01	2.84E+01
	γ_2	5.54E−02	5.23E−02	4.83E−02	4.36E−02	3.84E−02	3.29E−02	2.70E−02	2.10E−02	1.48E−02	8.54E−03
0-1	Dia.	a	c	c	c	a	a	a	a	a	a
Set *B*	β	2.28E+01	2.35E+01	2.41E+01	2.48E+01	2.54E+01	2.61E+01	2.68E+01	2.74E+01	2.81E+01	2.87E+01
	γ_2	4.61E−02	4.27E−02	3.88E−02	3.45E−02	3.00E−02	2.52E−02	2.03E−02	1.53E−02	1.02E−02	4.98E−03
0-2	Dia.	d	d	d	d	d	e	e	e	e	c
Set *C*	β	1.99E+01	2.09E+01	2.19E+01	2.29E+01	2.39E+01	2.49E+01	2.59E+01	2.69E+01	2.79E+01	2.89E+01
	γ_2	6.25E−02	6.01E−02	5.58E−02	5.02E−02	4.39E−02	3.70E−02	2.97E−02	2.21E−02	1.43E−02	6.31E−03
0-1	Dia.	*	*	*	a	a	a	a	a	a	a
Set *C*	β	2.10E+01	2.19E+01	2.28E+01	2.36E+01	2.45E+01	2.54E+01	2.63E+01	2.72E+01	2.80E+01	2.89E+01
	γ_2	5.71E−02	5.39E−02	4.96E−02	4.44E−02	3.86E−02	3.24E−02	2.60E−02	1.93E−02	1.24E−02	5.48E−03
0-2	Dia.	*	*	*	e	e	c	a	a	a	a

(of both types) occur between $\gamma_2 = 0.0625$ and $\gamma_2 = 0.057$, and further analysis will be needed to understand the complicated behavior in this region.

5.2.1. Examples: Six-dimensional Hopf–Hopf mode interactions. To demonstrate how the results in Table 5.1 were obtained we provide in Table 5.2 numerical values of the parameters for $m = 0$, $m = 1$ Hopf-Hopf interaction points from each of the three sets. Also appearing in the table are values of the normal form coefficients and values (derived from the normal form coefficients) of the stability-determining quantities described in § 3. Using these quantities and the information in Table 3.2 it is not difficult, although somewhat tedious, to derive the bifurcation diagram for each of the six-dimensional Hopf-Hopf interaction curves resulting in the information in Table 5.1. We note that several degeneracies appeared in Table 5.1. Some are potentially quite interesting, but remain to be analyzed.

5.3. Eight-dimensional Hopf–Hopf interactions and stable $m = 2$ rotating waves. Establishing stable $m = 2$ periodic solutions is a more difficult task. For sets B and C there are small regions where the $m = 2$ Hopf point is the primary bifurcation point, and for set C the results of [Golubitsky and Roberts, 1987] can be used to show that stable $m = 2$ rotating waves exist in this region. This may not be true for set B because the $m = 2$ standing and rotating waves both bifurcate subcritically in the region where the $m = 2$ Hopf point is the primary bifurcation point, and the degenerate $O(2)$ Hopf curves where they become supercritical never intersect this region. Thus the local

TABLE 5.2
Sample numerical values for the six-dimensional Hopf-Hopf interactions.

	x	y	λ	γ_2	β	ω_1	ω_2
A	7.06E−01	1.52E−02	2.78E−02	1.71E−02	5.02E+01	1.28E−02	1.49E−02
B	7.01E−01	3.77E−02	7.59E−02	4.83E−02	2.28E+01	5.66E−02	5.87E−02
C	6.39E−01	3.69E−02	6.00E−02	3.70E−02	2.49E+01	8.64E−02	8.70E−02

	$p_{0,\lambda}$	$p_{0,\beta}$	p_{00}	p_{01}	$p_{1,\lambda}$	$p_{1,\beta}$	p_{10}
A	5.03E+01	5.25E−01	−1.28E+01	−7.72E+00	4.69E+01	4.84E−01	−1.07E+01
B	9.77E+00	1.83E−01	−6.70E−01	−4.96E−01	9.51E+00	1.78E−01	−5.67E−01
C	4.89E+00	4.70E−02	−1.07E+00	−2.03E+00	4.81E+00	4.56E−02	−9.98E−01

	p_{11}	p_{12}
A	−1.79E+00	−1.43E+00
B	1.28E−01	−3.38E−01
C	−4.39E−01	−9.74E−01

	ε_{11}	ε_{21}	ε_{31}	ε_{12}	ε_{22}	ε_{32}	ε_{13}
A	−1.28E+01	1.20E+00	1.20E+00	−1.79E+00	3.57E−01	−5.80E+00	−3.22E+00
B	−6.70E−01	8.53E−02	8.53E−02	1.28E−01	−4.67E−01	−6.28E−01	−2.10E−01
C	−1.07E+00	5.79E−02	5.79E−02	−4.39E−01	−5.35E−01	−1.59E+00	−1.41E+00

	ε_{23}	ε_{33}	$\varepsilon_{\lambda\beta}$	det 4	det 6	diagram
A	−3.57E−01	−1.20E+01	−4.20E−03	−6.00E+01	−1.25E+02	f
B	4.67E−01	−7.76E−01	−6.04E−04	−3.67E−01	−4.22E−01	c
C	5.35E−01	−2.63E+00	−6.10E−04	−1.56E+00	−2.54E+00	a

methods of this paper are not conclusive for set B, but only suggest that the $m=2$ rotating waves turn around and become stable.

Further analysis depends on the eight-dimensional Hopf interaction. The results in Tables 3.5 and 3.6 can be used to construct partial bifurcation diagrams near the eight-dimensional interaction curves from the values of the normal form coefficients. The diagrams are partial because we have neglected to include information on the two standing wave branches. However, it turns out that the quantities ε_{22} and ε_{23} are always positive so the standing waves and their secondary branches are unstable. Example results are given in Table 5.3.

All we can say about set B is that if the $m=2$ rotating waves become stable after the limit point as we conjectured above, then they are likely to remain stable when the $m=1$ Hopf point is the primary bifurcation point. This follows because the secondary bifurcations on branch 4 occur for $\beta>0$ and ε_{24}, ε_{34}, and ε_{44} are all negative. The situation for set C is better because ε_{14} becomes negative and the $m=2$ rotating waves bifurcate supercritically. In fact, the results in Table 3.6 can be used to show that near the eight-dimensional interaction curve with $\gamma_2<0.0229$ the $m=2$ rotating waves become stable when the $m=1$ Hopf point is the primary bifurcation, and vice versa for the $m=1$ rotating waves when $m=2$ bifurcates first. Furthermore, on either side of the interaction curve there are values of λ for which the $m=1$ and $m=2$ rotating waves are simultaneously stable.

TABLE 5.3
Sample numerical values for the eight-dimensional Hopf–Hopf interaction.

	x	y	λ	γ_2	β	ω_1	ω_2
B	6.20E−01	3.17E−02	4.78E−02	1.78E−03	2.91E+01	7.02E−02	7.39E−02
C	5.92E−01	3.30E−02	4.63E−02	2.30E−03	2.93E+01	8.71E−02	8.88E−02
	$p_{1,\lambda}$	$p_{1,\beta}$	p_{11}	p_{12}	p_{13}	p_{14}	$p_{3,\lambda}$
B	4.40E+00	4.18E−02	−3.79E−01	−1.09E+00	7.33E−02	−6.31E−01	4.25E+00
C	4.73E+00	2.26E−02	−8.54E−01	−1.69E+00	−1.46E+00	−1.39E+00	4.61E+00
	$p_{3,\beta}$	p_{31}	p_{32}	p_{33}	p_{34}		
B	3.59E−02	−1.23E−01	−8.16E−01	6.02E−01	−4.45E−01		
C	1.98E−02	−1.33E+00	−1.36E+00	−5.17E−01	−1.04E+00		
	ε_{11}	ε_{21}	ε_{31}	ε_{41}	ε_{12}	ε_{22}	ε_{32}
B	−8.12E−01	−7.29E−01	2.21E−01	−4.58E−01	3.08E+00	1.46E+00	4.70E−01
C	−1.71E+00	−8.36E−01	−5.01E−01	−5.22E−01	−5.09E+00	1.67E+00	−2.07E−01
	ε_{42}	ε_{13}	ε_{23}	ε_{33}	ε_{34}	ε_{14}	ε_{24}
B	4.70E−01	1.08E−01	2.10E+00	−7.52E−01	−7.52E−01	1.10E+00	1.05E+00
C	−2.07E−01	−3.11E+00	1.04E+00	−1.25E+00	−1.25E+00	−1.03E+00	−5.20E−01
	ε_{33}	ε_{44}	$\varepsilon_{\lambda\beta}$	det 7	det 8		
B	1.26E+00	−5.76E−01	−4.49E−03	−9.01E−01	−3.24E+00		
C	−8.56E−01	−9.32E−01	−2.20E−03	−6.03E+00	−5.75E+00		

Now we can use the results in Table 5.1 for the set $C\,m=0$, $m=2$ six-dimensional interaction to conjecture that if $\gamma_2<0.0229$ the $m=2$ rotating waves remain stable when mode 2 bifurcates after both modes 0 and 1. The results in Table 5.1 are certainly consistent with this picture, but local bifurcation theory cannot be used to prove that it actually happens. That is, local bifurcation theory only provides a neighborhood of the eight-dimensional interaction curve where stable $m=2$ rotating waves exist; it does not guarantee that the neighborhood extends as far as the $m=0$, $m=2$ interaction curve. Such a result could be obtained via local bifurcation theory it we could bring all three modes together simultaneously, but this does not seem to happen in this model.

Appendix. In this section we describe the details of the normal form reductions for the various Hopf bifurcations and Hopf-Hopf mode interactions. We begin by considering the problem of computing the normal form for bifurcations of reaction-diffusion equations invariant under the action of the compact Lie group $O(2)$, although our methods would apply more generally. We then show, using group-theoretic results from [Golubitsky, Stewart, and Schaeffer, 1988], [Elphick et al., 1987], and [Chossat and Golubitsky, 1987] that if the eigenvalues of the center subspace are semisimple the problem of computing the normal form can be simplified because, in this case, the homological operator used in computing the normal form acts diagonally in a certain sense to be made precise below. These considerations, and some formal multivariable calculus results, finally lead us to an algorithm for generating formulas for the normal form coefficients based on elementary combinatorics. The advantages of this algorithm are that it eliminates errors in deriving the formulas and is suitable for computer implementation. We demonstrate the method by deriving some of the formulas used to obtain the results presented in § 5.

We assume that the reader is familiar with the material in [Guckenheimer and Holmes, 1983] and [Elphick et al., 1987], but, in general terms, the idea is that the local behavior of a complicated system can be determined near a bifurcation point by studying the behavior of a reduced set of ordinary differential equations, called the normal form, because it depends only on the type of bifurcation and can be studied independently of the original model, leading to a classification of the types of behavior that can occur near this bifurcation. Computing the coefficients in the normal form at a bifurcation point for a particular model enables us to take advantage of the general analysis of the normal form and to identify the behavior of the original system.

Our approach is specifically intended for numerical implementation of center manifold/normal form calculations. For this reason there are certain differences between our approach and the usual one for performing center manifold/normal form calculations by hand [Guckenheimer and Holmes, 1983] or with the aid of symbolic manipulators [Rand and Armbruster, 1987]. Simply stated, the more classical approach consists of three steps: (1) a change of coordinates is performed to bring the system into block-diagonal form; (2) the reduced vector field on the center manifold is computed; (3) the reduced vector field on the center manifold is brought into normal form. In the numerical approach we are using, step 1 is not performed and steps 2 and 3 are combined. This seems to offer calculational advantages that will beome more important as the size of the system grows. We hasten to state that these are not really new ideas; our adaptation and implementation of the ideas in the method of [Elphick et al., 1987] is similar in many ways to the method of alternative problems, or, in its more formalized form, the Lyapunov-Schmidt method, but it is also important to note that we are doing a center manifold/normal form reduction so stability information is maintained in a rigorous way. What is new in our approach is an algorithm based

on combinatorics for deriving the formulas for the normal form coefficients. Potentially, this algorithm could be programmed so that the expended formulas would never need to be written down; the program would be responsible for the expansions.

Consider a set of reaction diffusion equations with distinguished bifurcation parameter λ

$$u_t = D\Delta u + f(u, \lambda; \alpha) \tag{A.1}$$

defined on a circularly symmetric, bounded domain with smooth boundary. Other examples of suitable domains are annuli and disks, but in this paper we will consider only the circle to simplify the calculations. We assume that for a fixed value of α the invariant steady-state solution $u = u_0$, $\lambda = \lambda_0$ is a bifurcation point, i.e., the linearization, L, of (A.1) about this point has eigenvalues with zero real part. Since we are considering only Hopf bifurcation, the invariant steady-state solution has a smooth local extension $u_0(\lambda, \alpha)$. Thus without loss of generality we can assume that (A.1) has a trivial solution $u_0(\lambda, \alpha) \equiv 0$. This assumption simplifies the presentation somewhat. The details of how to do this locally are described in [Farr, Labouriau, and Langford, 1989].

The underlying function space for our analysis is the Hilbert space $\mathbf{H}$ of Fourier series with values in $\mathbf{R}^n$, using the inner product given by composing the standard inner product in $\mathbf{R}^n$ with the standard L^2 inner product. (In our calculations it will be convenient to use complex Fourier series with the obvious change in the inner product.) Thus by standard theorems [Henry, 1981] we can write $\mathbf{H} = E \oplus W$, where E is the (finite-dimensional) critical eigenspace and the eigenvalues of $L|_W$ have nonzero real part. (To obtain stable solutions from the reduction they must have negative real part.) For the singularities we are interested in, dim (E) is even, so let dim $(E) = 2p$. Furthermore, it is quite easy to show that the operator L is sectorial, which is a technical condition needed to apply the center manifold theorem [Henry, 1981].

Complex coordinates for E are the most natural for Hopf bifurcation because the action takes a particularly simple form. For example, for an $m = 1$ symmetry-breaking Hopf bifurcation any solution of the linearized equation $v_t = Lv$ can be written in the form

$$z_1 c\, e^{i(\psi+\omega t)} + z_2 c\, e^{i(\omega t-\psi)} + \bar{z}_1 \bar{c}\, e^{-i(\psi+\omega t)} + \bar{z}_2 \bar{c}\, e^{i(\psi-\omega t)}, \tag{A.2}$$

where c is the appropriate eigenvector as in (2.4) and $(z_1, z_2) \in C^2$. The reader can check that the action of $O(2)$ given in (2.2) and a phase shift, after rescaling time, generate the action of $O(2) \times S^1$ claimed in § 3 on (z_1, z_2). For the reduction we make the amplitudes time dependent and write, using the eigenfunctions of L,

$$Y = z_1 c\, e^{i\psi} + z_2 c\, e^{-i\psi} + \bar{z}_1 \bar{c}\, e^{-i\psi} + \bar{z}_2 \bar{c}\, e^{i\psi}, \tag{A.3}$$

but retain the S^1 action on (z_1, z_2). For the other singularities of interest, similar expressions of the form

$$Y = z_1 \phi_1 + \cdots + z_p \phi_p + \text{complex conjugate} \tag{A.4}$$

can be written down, where ϕ_i is an eigenfunction of $L|_E$, so we will identify Y with the complex coordinates $(z_1, \cdots, z_p)$ where $p = 2$ for symmetry-breaking Hopf bifurcation and $p = 3$ or $p = 4$ for the mode interactions. We also let $(\mu_1, \cdots, \mu_p, \mu_{p+1}, \cdots, \mu_{2p})$ be the eigenvalues of $L|_E$ written in the proper order so that $L\phi_i = \mu_i \phi_i$, $i = 1, p$, and $\mu_{p+j} = \bar{\mu}_j$, $j = 1, p$. Following [Elphick et al., 1987] we introduce a projection $P_0 : \mathbf{H} \to E$, which commutes with L. This can be done in a standard way by using the eigenfunctions of L^*, the adjoint of L.

The center manifold/normal form reduction begins by substituting $u = Y + \Psi(Y)$ into (A.1) to obtain

$$\dot{Y} + d\Psi \cdot \dot{Y} = d\Delta(Y + \Psi) + f(Y + \Psi, \lambda; \alpha). \tag{A.5}$$

The formal normal form equation is

$$\dot{Y} = F(Y, \lambda; \alpha) \tag{A.6}$$

and the idea is to find the simplest possible form for (A.6). Let A be the matrix representing L on the coordinates Y for E. Then [Elphick et al., 1987] show that in the semisimple eigenvalue case F can be chosen to commute with the group $\mathbf{S}$ generated by $\exp(At)$. In the case of Hopf bifurcation or Hopf–Hopf mode interactions, [Golubitsky and Stewart, 1985] and [Chossat, Golubitsky, and Keyfitz, 1986] show that $\mathbf{S}$ is isomorphic to the torus $\mathbf{T}^j$ for some j. If the partial differential equation (PDE) (A.1) also commutes with the action of a compact group Γ ($= O(2)$ in our case) then these results and those in [Elphick et al., 1987] combine to show that F can be chosen to commute with $\Gamma \times \mathbf{S}$.

In practice a Taylor series approximation ot Ψ is calculated to obtain the truncated normal form. As we will see below, computing this expansion for Ψ proceeds by defining a projection P and solving a series of nonhomogeneous linear problems. By writing the right-hand sides of (A.1) and (A.6) as $Lu + \tilde{f}(u, \lambda; \alpha)$ and $AY + \tilde{F}(Y, \lambda; \alpha)$, equation (A.5) can be rearranged into the more standard form

$$L\Psi - d\Psi \cdot AY = \tilde{F}(Y, \lambda; \alpha) + d\Psi \cdot \tilde{F}(Y, \lambda; \alpha) - \tilde{f}(u_0 + Y + \Psi, \lambda; \alpha) \tag{A.7}$$

where the linear operator, $L\Psi - d\Psi \cdot AY$, on the left-hand side of (A.7) is a Lie bracket often abbreviated as ad_L in the literature [Elphick et al., 1987]. It is proven in [Ruelle, 1973] that the mapping Ψ can be constructed to be invariant under Γ, but this follows in the present case from the simpler considerations detailed below. The procedure of [Elphick et al., 1987] is to use the projection P_0 to split (A.4) into two equations. It turns out, however, that in the case of semisimple eigenvalues there is a more convenient projection that simplifies the calculations. This projection will be developed below, after we introduce some background material.

A convenient notation for the Taylor coefficients of Ψ is given by

$$\Psi = \sum_{|\alpha| \geqq 2} \frac{z^\alpha}{\alpha!} \Psi_\alpha, \tag{A.8}$$

where $\alpha = (\alpha_1, \cdots, \alpha_p, \alpha_{p+1}, \cdots, \alpha_{2p})$ is a multi-index and

$$z^\alpha = z_1^{\alpha_1} \cdots z_p^{\alpha_p} \bar{z}_1^{\alpha_{p+1}} \cdots \bar{z}_p^{\alpha_{2p}}. \tag{A.9}$$

The coefficients Ψ_α take values in $\mathbf{H}$, so they have Fourier series. It will be shown below that the action of $O(2)$ on them can be determined by its action on z. More precisely, it comes from tensor products of the action, as was shown by [Sattinger, 1979] for the similar Lyapunov–Schmidt reduction. In practice this means that

$$\Psi_\alpha(\psi) = \hat{\Psi}_\sigma e^{in(\alpha)\psi}, \tag{A.10}$$

that is, only a single Fourier mode contributes. For example, for a mode m $O(2)$ Hopf bifurcation $n(\alpha) = m(\alpha_1 - \alpha_2 - \alpha_3 + \alpha_4)$. Since the value of n is determined by m and α, we will often use Ψ_α and $\hat{\Psi}_\alpha$ interchangeably.

Now, let $P_k(O(2))$ be the space of homogeneous polynomial maps in z of degree k, $k \geqq 2$, with values in $\mathbf{H}$ generated by terms of the form $z^\alpha \Psi_\alpha$, where Ψ_α satisfies (A.10). We further require that the maps be invariant under $O(2)$. It is easy to check

that this is a finite-dimensional space. It turns out that by exploiting the compactness of $\mathbf{S}$ we can construct a projection P that simplifies the calculations. The requirements on P in [Elphick et al., 1987] are that it is a projection onto E and that it commutes with L. Since the actual calculations take place in $P_k(O(2))$, we can obtain a useful projection as follows. Let P_0 be the projection onto E. The action of $O(2)\times\mathbf{S}$ on the critical eigenfunctions spanning E generates an action of $O(2)\times\mathbf{S}$ on the coordinates z ($\approx \mathbf{C}^p$ where $\dim(E)=2p$) we have chosen on E. Let $P_k^E(O(2)\times\mathbf{S}))$ be the subspace of $P_k(O(2))$, which has values in E and is equivariant under the action of $O(2)\times\mathbf{S}$. Since $\mathbf{S}$ is compact, it is a general result [Rudin, 1973] that there exists a unique normalized Haar measure, denoted $d\sigma$, on $\mathbf{S}$. It is trivial to generalize on a result proven in [Golubitsky, Stewart, and Schaeffer, 1988, Lemma 5.10, p. 292] to show that $\rho: P_k(O(2))\to P_k^E(O(2)\times\mathbf{S})$ defined by

$$\rho(\Psi)=\int_{\mathbf{S}}\sigma^{-1}P_0\Psi(\sigma\cdot z)\,d\sigma \tag{A.11}$$

is a linear projection.

Now the results in [Elphick et al., 1987] and [Golubitsky, Stewart, and Schaeffer, 1988] can be used to see that

$$\begin{aligned}&\ker(ad_L)=P_k^E(O(2)\times\mathbf{S}),\\ &P_k(O(2))=P_k^E(O(2)\times\mathbf{S})\oplus ad_L(P_k(O(2))).\end{aligned} \tag{A.12}$$

Thus if we use ρ for the projection and require $\rho\Psi=0$, (A.7) can be split into the two equations:

$$0=\tilde{F}(Y,\lambda;\alpha)-\rho\tilde{f}(Y+\Psi,\lambda;\alpha), \tag{A.13a}$$

$$ad_L(\Psi)=-(1-\rho)\tilde{f}(Y+\Psi,\lambda;\alpha)+d\Psi\cdot\rho\tilde{f}(Y+\Psi,\lambda;\alpha). \tag{A.13b}$$

In practice the integral over $\mathbf{S}$ in (A.11) can be done analytically because it reduces to a complex Fourier series calculation, and well-known orthogonality relations can be used. For example, for a mode m Hopf bifurcation the group $\mathbf{S}$ is just $\mathbf{S}^1$ and the action of $\phi\in\mathbf{S}^1$ on $z^\alpha\Psi_\alpha$ is

$$\phi\cdot(z^\alpha\Psi_\alpha)=e^{ip(\alpha)\phi}z^\alpha\Psi_\alpha, \tag{A.14}$$

where $p(\alpha)=\alpha_1+\alpha_2-\alpha_3-\alpha_4$. For each of the Hopf–Hopf mode interactions, there are two phase variables (ϕ_1,ϕ_2) and two functions $p_1(\alpha)$ and $p_2(\alpha)$. Thus in the $O(2)$ Hopf case, $p(\alpha)\neq\pm1$ means $\rho(z^\alpha\Psi_\alpha)=0$ so for many terms in the series for Ψ the projection ρ is trivial to compute. If $p(\alpha)=\pm1$ then the projection P_0 is important and more care is needed. However, the $O(2)$ invariance of Ψ and the original PDE in (A.1) also simplify this procedure, as we will see below.

Calculation of the normal form coefficients proceeds by expanding the terms in (A.13) in a Taylor series and equating coefficients. It is clear from the equations that we could begin by computing all of the quadratic terms and then move up to the cubic terms, etc., but this is not the most efficient procedure. On the contrary, much needless computation can be avoided by starting at the highest order and determining precisely which lower-order terms are needed. Symmetry can also be used to reduce the calculation effort. For example, for symmetry-breaking $O(2)$ Hopf calculations up to seventh order, the savings in minimizing the number of terms in Ψ that must be computed are detailed in Table A.1. To show more concretely how symmetry is useful, we show in Table A.2 the ten quadratic terms in the expansion of Ψ for an $m=1$ Hopf bifurcation and the relationships that reduce the number of distinct coefficients to four. Using the

TABLE A.1
Calculational savings for $O(2)$ Hopf bifurcation.

Order	Possible terms	Minimum terms	Required terms
2	10	4	4
3	20	5	5
4	35	11	11
5	56	14	9
6	?	26	9

TABLE A.2
Quadratic expansion of Ψ, top, and relations between coefficients, bottom.

$$\tfrac{1}{2}z_1^2\hat{\Psi}_{2000}\,e^{2i\psi}+z_1\bar{z}_1\hat{\Psi}_{1010}+z_1z_2\hat{\Psi}_{1100}+z_1\bar{z}_2\hat{\Psi}_{1001}\,e^{2i\psi}+\tfrac{1}{2}z_2^2\hat{\Psi}_{0200}\,e^{-2i\psi}+z_2\bar{z}_2\hat{\Psi}_{0101}+\tfrac{1}{2}\bar{z}_1^2\hat{\Psi}_{0020}\,e^{-2i\psi}$$
$$+\bar{z}_1\bar{z}_2\hat{\Psi}_{0011}+\bar{z}_1z_2\hat{\Psi}_{0110}\,e^{-2i\psi}+\tfrac{1}{2}\bar{z}_2^2\hat{\Psi}_{0002}\,e^{2i\psi}$$

$$\hat{\Psi}_{0200}=\hat{\Psi}_{2000}\qquad \hat{\Psi}_{0101}=\hat{\Psi}_{1010}\qquad \hat{\Psi}_{0020}=\hat{\Psi}_{2000}\qquad \hat{\Psi}_{0011}=\hat{\Psi}_{1100}\qquad \hat{\Psi}_{0110}=\hat{\Psi}_{1001}\qquad \hat{\Psi}_{0002}=\hat{\Psi}_{2000}$$

remark after (A.10), the reader can verify that the Fourier modes shown are the correct ones. It is generally true even Fourier modes appear at even orders and conversely at odd orders.

We now show how to organize the equating of Taylor coefficients in the expansion of (A.13) so that elementary combinatorics can be used to generate correct formulas for numerical evaluation. This approach rests on some simple formal results in multivariable calculus and a convenient shorthand notation. Suppose we let $G(Y)=f(Y+\Psi(Y))$, where $f(\cdot)$ is as in (A.5), Y is as in (A.4), Ψ begins with quadratic terms, and we have suppressed the parameter dependence of f for simplicity. Then the derivatives of G up to fifth order evaluated at $Y=0$ are given by

$$\begin{aligned}
dG &= dF,\\
d^2G &= df\cdot d^2\Psi + d^2f,\\
d^3G &= df\cdot d^3\Psi + 3d^2f(I, d^2\Psi) + d^3f,\\
d^4G &= df\cdot d^4\Psi + 4\,d^2f(I, d^3\Psi) + 6\,d^3f(I, I, d^2\Psi)\\
&\quad + 3\,d^2f(d^2\Psi, d^2\Psi) + d^4f,\\
d^5G &= dF\cdot d^5\Psi + 5\,d^2f(I, d^4\Psi) + 10\,d^3f(I, I, d^3\Psi)\\
&\quad + 10\,d^2f(d^2\Psi, d^3\Psi) + 15\,d^3f(I, d^2\Psi, d^2\Psi)\\
&\quad + 10\,d^4f(I, I, I, d^2\Psi) + d^5f.
\end{aligned} \tag{A.15}$$

The formal computations used to derive (A.15) are straightforward, but the notation needs explaining. By d^kG we mean the symmetric k-linear form, which acts on k vectors $v_1, \cdots, v_k$. To simplify the expressions appearing in (A.15) we have used the following convention. A term like $d^2f(I, d^2\Psi)$ must act on three vectors v_1, v_2, v_3 and be invariant under permutations of the vectors. Hence we define this action to be

$$\begin{aligned}
3\,d^2f(I, d^2\Psi)(v_1, v_2, v_3) &\equiv d^2f(v_1, d^2\Psi(v_2, v_3))\\
&\quad + d^2f(v_2, d^2\Psi(v_1, v_3))\\
&\quad + d^2f(v_3, d^2\Psi(v_1, v_2)),
\end{aligned} \tag{A.16}$$

that is, all permutations of v_1, v_2, v_3, which leads to distinct terms. The letter I stands for the identity operator, and the integer coefficients preceding terms give the number of distinct terms. These coefficients can be obtained from elementary combinatorics, using binomial and multinomial coefficients, by treating it as the problem of dividing k distinct objects, $v_1, \cdots, v_k$, into groups. A slight complication arises for terms like $d^3f(I, d^2\Psi, d^2\Psi)$ when some of the groups may themselves be permuted, but this is easily dealt with by dividing by the number of such permutations. An advantage of taking this point of view is that in actual calculations the vectors $v_1, \cdots, v_k$ are often not distinct but themselves consist of several groups, with each element in a group being identical. In this case it is not necessary to write out the full expansion as in (A.16). Rather, we can employ combinatorics to determine only the distinct terms and their multiplicities. As an example to clarify these ideas, we will present formulas below for one of the fifth-order $O(2)$ Hopf coefficients.

Before doing so, we need another formal calculus result. Let $\Psi(Y)$ be as above, $F\colon E \to E$, and $H(Y) = d\Psi \cdot F(Y)$. Then the derivatives up to fifth order of H evaluated at $Y = 0$ are given by

$$
\begin{aligned}
dH &= d^2\Psi(I, F) + d\Psi \cdot dF,\\
d^2H &= d^3\Psi(I, I, F) + 2\, d^2\Psi(I, dF) + d\Psi \cdot d^2F,\\
d^3H &= d^4\Psi(I, I, I, F) + 3\, d^3\Psi(I, I, dF) + 3\, d^2\Psi(I, d^2F) + d\Psi \cdot d^3F,\\
d^4H &= d^5\Psi(I, I, I, I, F) + d\, d^4\Psi(I, I, I, dF) + 6\, d^3\Psi(I, I, d^2F)\\
&\quad + 4\, d^2\Psi(I, d^3F) + d\Psi \cdot d^4F,\\
d^5H &= d^6\Psi(I, I, I, I, I, F) + 5\, d^5\Psi(I, I, I, I, dF) + 10\, d^4\Psi(I, I, I, d^2F)\\
&\quad + 10\, d^3\Psi(I, I, d^3F) + 5\, d^2\Psi(I, d^4F) + d\Psi \cdot d^5F,
\end{aligned}
\tag{A.17}
$$

using the same convention as in (A.16).

As an application of (A.17), let Ψ be in $P_k(O(2))$ and $|\alpha| = k$, $k \leqq 5$. It is a simple calculation to see that

$$
d^\alpha(d\Psi \cdot AY)\big|_{Y=0} = \alpha \cdot \mu \Psi_a, \tag{A.18}
$$

where $\alpha \cdot \mu = \alpha_1\mu_1 + \cdots + \alpha_{2p}\mu_{2p}$. This result was noted much earlier in the context of ordinary differential equations in [Arnold, 1983]. The importance for our work is that it implies that ad_L acts diagonally on each term in the Taylor series for Ψ. As an aside we note that it can also be used to provide a direct, but inelegant proof of (A.12). Furthermore, (A.18) can be generalized to any singularity with semisimple critical eigenvalues.

To illustrate the technique, we derive formulas for one of the fifth-order coefficients of the $m = 1$ $O(2)$ Hopf normal form (3.3). We choose the term $z_1^2\bar{z}_1z_2\bar{z}_2$, which appears in the $\dot{z}_1$ equation of (3.3) because it is the most difficult of the three fifth-order coefficients. Suppose that c and ω are as in (A.3) and that c has been normalized so that $|c| = 1$. Write $L = D\Delta + B$, where B is the Jacobian matrix of f at the bifurcation point. Let d satisfy $(B^t - D)d = -i\omega\, d$, that is, $d\, e^{i\psi}$ is an eigenfunction of L^* with eigenvalue $-i\omega$. Assume that $d^* \cdot c = 1$, where d^* is the conjugate transpose of d. Let $v(\psi) \in \mathbf{H}$. Then the first component of the projection P_0v is given by

$$
\frac{1}{2\pi}\int_0^{2\pi} e^{-i\psi}\, d^* \cdot v(\psi)\, d\psi. \tag{A.19}
$$

To obtain the fifth-order coefficient that we want, we must compute the first component

of $\rho(d^5G(\phi_1, \phi_1, \bar{\phi}_1, \phi_2, \bar{\phi}_2))$ where the ϕ_i's are as in (A.4) and $G(Y)=f(Y+\Psi(Y))$. If we substitute into the last equation of (A.15) and assume that (A.10) holds, we will show below that there is a factor of $e^{i\psi}$ multiplying the whole expression, so there is no need to carry along factors of $e^{i\psi}$ in our calculation. We do, however, need to distinguish between the four eigenfunctions in our calculations so we use c_1, c_2, $\bar{c}_1$, $\bar{c}_2$ in deriving the formula. Remember in evaluating them that $c_1=c_2=c$ and $\bar{c}_1=\bar{c}_2=\bar{c}$. The result of making this substitution and expanding the right-hand side is shown in Table A.3. The coefficient we want can now be calculated using (A.19) as $d^*\cdot$ (expression in Table A.3).

From Table A.3 we can pick out all of the terms in the expansion of Ψ that we need. Using symmetry as before, we can choose a minimal set that must be calculated. One such choice is given in Table A.4. (Additional terms are needed to calculate the other two fifth-order coefficients.) We need all four of the quadratic terms, but considering one of them in detail will serve to illustrate the procedure. Ψ_{2000}, for example, is obtained by solving

$$(L-2i\omega I)\Psi_{2000}=-d^2f(c\,e^{i\psi}, c\,e^{i\psi}) \tag{A.20}$$

but, by using the bilinearity of d^2f, we can factor out $e^{2i\psi}$ on the right-hand side and get

$$(L-2i\omega I)\Psi_{2000}=-e^{2i\psi}\,d^2f(c, c), \tag{A.21}$$

which shows that (A.10) is satisfied for this particular term. The reader can easily verify that (A.10) is satisfied for all of the other quadratic terms and that the relations shown in Table A.2 are correct. Verifying that (A.10) holds to any finite order of expansion now proceeds easily by induction.

Equation (A.21) can also be written in the form

$$(B-4D-2i\omega I)\Psi_{2000}=-d^2f(c, c). \tag{A.22}$$

TABLE A.3
Expanded form of $D^5G(\phi_1, \phi_1, \bar{\phi}_1, \phi_2, \bar{\phi}_2)$.

$$\begin{aligned}
&2D^2f(c_1, \hat{\Psi}_{1111})+D^2f(\bar{c}_1, \hat{\Psi}_{2101})+D^2f(c_2, \hat{\Psi}_{2011})+D^2f(\bar{c}_2, \hat{\Psi}_{2110})+D^3f(c_2, \bar{c}_2, \hat{\Psi}_{2010})+D^3f(\bar{c}_1, \bar{c}_2, \hat{\Psi}_{2100})\\
&\quad+D^3f(\bar{c}_1, c_2, \hat{\Psi}_{2001})+2D^3f(c_1, \bar{c}_2, \hat{\Psi}_{1110})+2D^3f(c_1, \bar{c}_1, \hat{\Psi}_{1101})+2D^3f(c_1, c_2, \hat{\Psi}_{1011})\\
&\quad+D^3f(c_1, c_1, \hat{\Psi}_{0111})+D^2f(\hat{\Psi}_{2010}, \hat{\Psi}_{0101})+D^2f(\hat{\Psi}_{2100}, \hat{\Psi}_{0011})+D^2f(\hat{\Psi}_{2001}, \hat{\Psi}_{0110})\\
&\quad+2D^2f(\hat{\Psi}_{1110}, \hat{\Psi}_{1001})+2D^2f(\hat{\Psi}_{1101}, \hat{\Psi}_{1010})+2D^2f(\hat{\Psi}_{1011}, \hat{\Psi}_{1100})+D^2f(\hat{\Psi}_{0111}, \hat{\Psi}_{2000})\\
&\quad+2D^3f(c_1, \hat{\Psi}_{1010}, \hat{\Psi}_{0101})+2D^3f(c_1, \hat{\Psi}_{1100}, \hat{\Psi}_{0011})+2D^3f(c_1, \hat{\Psi}_{1001}, \hat{\Psi}_{0110})+D^3f(\bar{c}_1, \hat{\Psi}_{2000}, \hat{\Psi}_{0101})\\
&\quad+2D^3f(\bar{c}_1, \hat{\Psi}_{1100}, \hat{\Psi}_{1001})+D^3f(c_2, \hat{\Psi}_{2000}, \hat{\Psi}_{0011})+2D^3f(c_2, \hat{\Psi}_{1010}, \hat{\Psi}_{1001})+D^3f(\bar{c}_2, \hat{\Psi}_{2000}, \hat{\Psi}_{0110})\\
&\quad+2D^3f(\bar{c}_2, \hat{\Psi}_{1010}, \hat{\Psi}_{1100})+D^4f(\bar{c}_1, c_2, \bar{c}_2, \hat{\Psi}_{2000})+2D^4f(c_1, c_2, \bar{c}_2, \hat{\Psi}_{1010})+2D^4f(c_1, \bar{c}_1, \bar{c}_2, \hat{\Psi}_{1100})\\
&\quad+2D^4f(c_1, \bar{c}_1, c_2, \hat{\Psi}_{1001})+D^4f(c_1, c_1, \bar{c}_2, \hat{\Psi}_{0110})+D^4f(c_1, c_1, c_2, \hat{\Psi}_{0011})+D^4f(c_1, c_1, \bar{c}_1, \hat{\Psi}_{0101})\\
&\quad+D^5f(c_1, c_1, \bar{c}_1, c_2, \bar{c}_2)
\end{aligned}$$

TABLE A.4

Order	Minimal set of Taylor coefficients
2	$\hat{\Psi}_{2000}, \hat{\Psi}_{1100}, \hat{\Psi}_{1010}, \hat{\Psi}_{1001}$
3	$\hat{\Psi}_{2100}, \hat{\Psi}_{2010}, \hat{\Psi}_{2001}, \hat{\Psi}_{1101}$
4	$\hat{\Psi}_{2110}, \hat{\Psi}_{2011}, \hat{\Psi}_{2101}, \hat{\Psi}_{1111}$

Thus computing the coefficients Ψ_α can be reduced to solving a series of finite-dimensional linear algebra problems. We note that for general values of m, the right-hand side takes the form

$$(A.23) \qquad (B-(n(\alpha))^2 D-\alpha\cdot\mu I)\Psi_\alpha.$$

Table A.5 presents the calculations for the remaining terms that we need in the expansion of Ψ. For the first and fourth third-order terms, the projection $I-\rho$ in (A.13b) does not act trivially. This is because $z_1^2\bar{z}_1$ and $z_1z_2\bar{z}_2$ are terms that appear in the first component of the normal form, so we have to subtract the component on the

TABLE A.5

Second-, third-, and fourth-order terms needed to compute the $z_1^2\bar{z}_1z_2\bar{z}_2$ fifth-order term in the $O(2)$ Hopf normal form.

Second-order terms

$$(B-4D-2i\omega I)\hat{\Psi}_{2000}=-D^2f(c_1,c_1)$$
$$(B)\hat{\Psi}_{1010}=-D^2f(c_1,\bar{c}_1)$$
$$(B-2i\omega I)\hat{\Psi}_{1100}=-D^2f(c_1,c_2)$$
$$(B-4D)\hat{\Psi}_{1001}=-D^2f(c_1,\bar{c}_1)$$

Third-order terms

$$(B-D-i\omega I)\hat{\Psi}_{2010}=-[2D^2f(c_1,\hat{\Psi}_{1010})+D^2f(\bar{c}_1,\hat{\Psi}_{2000})+D^3f(c_1,c_1,\bar{c}_1)]$$
$$+\{d^*\cdot[2D^2f(c_1,\hat{\Psi}_{1010})+D^2f(\bar{c}_1,\hat{\Psi}_{2000})+D^3f(c_1,c_1,\bar{c}_1)]\}c_1,\ d^*\cdot\hat{\Psi}_{2010}=0$$
$$(B-D-3i\omega I)\hat{\Psi}_{2100}=-[2D^2f(c_1,\hat{\Psi}_{1100})+D^2f(c_2,\hat{\Psi}_{2000})+D^2f(c_1,c_1,c_2)]$$
$$(B-9D-i\omega I)\hat{\Psi}_{2001}=-[2D^2f(c_1,\hat{\Psi}_{1001})+D^2f(\bar{c}_2,\hat{\Psi}_{2000})+D^2f(c_1,c_1,\bar{c}_2)]$$
$$(B-D-i\omega I)\hat{\Psi}_{1101}=-[D^2f(c_1,\hat{\Psi}_{0101})+D^2f(c_2,\hat{\Psi}_{1001})+D^2f(\bar{c}_2,\hat{\Psi}_{1100})+D^3f(c_1,c_2,\bar{c}_2)]$$
$$+\{d^*\cdot[D^2f(c_1,\hat{\Psi}_{0101})+D^2f(c_2,\hat{\Psi}_{1001})+D^2f(\bar{c}_2,\hat{\Psi}_{1100})$$
$$+D^3f(c_1,c_2,\bar{c}_2)]\}c_1,\ d^*\cdot\hat{\Psi}_{1101}=0$$

Fourth-order terms

$$(B-2i\omega I)\hat{\Psi}_{2110}=-[2D^2f(c_1,\hat{\Psi}_{1110})+D^2f(\bar{c}_1,\hat{\Psi}_{2100})+D^2f(c_2,\hat{\Psi}_{2010})+D^3f(\bar{c}_1,c_2,\hat{\Psi}_{2000})$$
$$+2D^3f(c_1,c_2,\hat{\Psi}_{1010})+2D^3f(c_1,\bar{c}_1,\hat{\Psi}_{1100})+D^3f(c_1,c_1,\hat{\Psi}_{0110})+D^2f(\hat{\Psi}_{2000},\hat{\Psi}_{0110})$$
$$+2D^2f(\hat{\Psi}_{1010},\hat{\Psi}_{1100})+D^4f(c_1,c_1,c_2,\bar{c}_1)]+(a+2b)\hat{\Psi}_{1100}$$
$$(B-4D)\hat{\Psi}_{2011}=-[2D^2f(c_1,\hat{\Psi}_{1011})+D^2f(\bar{c}_1,\hat{\Psi}_{2001})+D^2f(\bar{c}_2,\hat{\Psi}_{2010})+D^3f(\bar{c}_1,\bar{c}_2,\hat{\Psi}_{2000})$$
$$+2D^3f(c_1,\bar{c}_2,\hat{\Psi}_{1010})+2D^3f(c_1,\bar{c}_1,\hat{\Psi}_{1001})+D^3f(c_1,c_1,\hat{\Psi}_{0011})+D^2f(\hat{\Psi}_{2000},\hat{\Psi}_{0011})$$
$$+2D^2f(\hat{\Psi}_{1010},\hat{\Psi}_{1001})+D^4f(c_1,c_1,\bar{c}_2,\bar{c}_1)]+(a+2\bar{b})\hat{\Psi}_{1100}$$
$$(B-4D-2i\omega I)\hat{\Psi}_{2101}=-[2D^2f(c_1,\hat{\Psi}_{1101})+D^2f(c_2,\hat{\Psi}_{2001})+D^2f(\bar{c}_2,\hat{\Psi}_{2100})+D^3f(c_2,\bar{c}_2,\hat{\Psi}_{2000})$$
$$+2D^3f(c_1,c_2,\hat{\Psi}_{1001})+2D^3f(c_1,\bar{c}_2,\hat{\Psi}_{1100})+D^3f(c_1,c_1,\hat{\Psi}_{0101})+D^2f(\hat{\Psi}_{2000},\hat{\Psi}_{0101})$$
$$+2D^2f(\hat{\Psi}_{1100},\hat{\Psi}_{1001})+D^4f(c_1,c_1,c_2,\bar{c}_2)]+2b\hat{\Psi}_{2000}$$
$$(B)\hat{\Psi}_{1111}=-[D^2f(c_1,\hat{\Psi}_{0111})+D^2f(\bar{c}_1,\hat{\Psi}_{1101})+D^2f(c_2,\hat{\Psi}_{1011})+D^2f(\bar{c}_2,\hat{\Psi}_{1110})+D^3f(c_2,\bar{c}_2,\hat{\Psi}_{1010})$$
$$+D^3f(\bar{c}_1,\bar{c}_2,\hat{\Psi}_{1100})+D^3f(\bar{c}_1,c_2,\hat{\Psi}_{1001})+D^3f(c_1,\bar{c}_2,\hat{\Psi}_{0110})+D^3f(c_1,c_2,\hat{\Psi}_{0011})$$
$$+D^2f(c_1,\bar{c}_1,\hat{\Psi}_{0101})+D^2f(\hat{\Psi}_{1010},\hat{\Psi}_{0101})+D^2f(\hat{\Psi}_{1100},\hat{\Psi}_{0011})+D^2f(\hat{\Psi}_{1001},\hat{\Psi}_{0110})$$
$$+D^4f(c_1,c_2,\bar{c}_1,\bar{c}_2)]+(b+\bar{b})[\hat{\Psi}_{1010}+\hat{\Psi}_{0101}],$$

where

$$a=d^*\cdot[2D^2f(c_1,\hat{\Psi}_{1010})+D^2f(\bar{c}_1,\hat{\Psi}_{2000})+D^3f(c_1,c_1,\bar{c}_1)]$$
$$b=d^*\cdot[D^2f(c_1,\hat{\Psi}_{0101})+D^2f(c_2,\hat{\Psi}_{1001})+D^2f(\bar{c}_2,\hat{\Psi}_{1100})+D^3f(c_1,c_2,\bar{c}_2)]$$

right-hand side, which is in $P_k^E((O(2)\times\mathbf{S})$, to solve the equation. The orthogonality conditions come from our requirements that $\rho\Psi=0$.

The fourth-order terms in Table A.5 also include contributions from the term $d\Psi\cdot\rho\tilde{f}(Y+\Psi,\bar{\lambda};\alpha)$ on the right-hand side of (A.13). As an example we consider the contribution this term makes to the equation for $\hat{\Psi}_{2011}$. The easiest way to see it is to recall from (A.13a) that $\tilde{F}(Y,\lambda;\alpha)=\rho\tilde{f}(Y+\Psi,\lambda;\alpha)$ and use the last line of (A.17) to obtain

$$\begin{aligned} d^4[d\Psi\cdot\tilde{F}](c_1,c_1,\bar{c}_1,c_2) &= 2\,d^2\Psi(c_1,d^3F(c_1,\bar{c}_1,c_2)) \\ &\quad + d^2\Psi(\bar{c}_1,d^3F(c_1,c_1,c_2)) \\ &\quad + d^2\Psi(c_2,d^3F(c_1,c_1,\bar{c}_1)). \end{aligned} \tag{A.24}$$

Note that all of the other terms vanish because Ψ and $\tilde{F}$ both begin with quadratic terms. Now the first and third terms on the right-hand side of (A.24) can be identified with cubic terms in the normal form, but the second term cannot, so it must vanish. With the aid of (A.13a) and the definitions of a and b in Table A.5, (A.24) becomes

$$d^4[d\Psi\cdot\tilde{F}](c_1,c_1,\bar{c}_1,c_2)=2b\,d^2\Psi(c_1,c_2)+d\,d^2\Psi(c_2,c_1), \tag{A.25}$$

and the entry in the table is verified.

So far we have not considered any parameter derivatives in our normal form calculations. Certain derivatives are needed, however, and we now briefly describe how this is done. For Hopf bifurcation, there are essentially two methods. In the first method, the eigenfunctions at the bifurcation point are replaced with their parameter-dependent extensions in a neighborhood of the bifurcation point. Using this method, we obtain parameter derivatives of the normal form coefficients by direct differentiation. For other singularities, these smooth extensions may not exist, so a more general method uses only the eigenfunctions at the bifurcation point, and equations for parameter derivatives of F and Ψ are obtained by differentiating (A.13). For example, to obtain λ derivatives the equations are

$$\begin{aligned} 0 &= d_\lambda\tilde{F}(Y,\lambda;\alpha)-\rho[d_u\tilde{f}(Y+\Psi,\lambda;\alpha)\cdot d_\lambda\Psi+d_\lambda\tilde{f}(Y+\Psi,\lambda;\alpha)], \\ ad_L(d_\lambda\Psi) &= -(I-\rho)[d_u\tilde{f}(Y+\Psi,\lambda;\alpha)\cdot d_\lambda\Psi+d_\lambda\tilde{f}(Y+\Psi,\lambda;\alpha)] \\ &\quad + d_Yd_\lambda\Psi\cdot\tilde{F}(Y,\lambda;\alpha)+d_Y\Psi\cdot d_\lambda\tilde{F}(Y,\lambda;\alpha). \end{aligned} \tag{A.26}$$

The methods used above still apply, but as the reader can imagine, the formulas rapidly become tedious to write out. The second equation can be used to show recursively that $d_\lambda^k\Psi|_{Y=0}=0$ for $k=1,2,\cdots$, so the parameter-dependent expansion for Ψ begins with $O(Y\lambda)$ terms.

REFERENCES

V. I. ARNOLD (1983), *Geometrical Methods in the Theory of Ordinary Differential Equations*, Springer-Verlag, New York.

J. F. G. AUCHMUTY (1979), *Bifurcating waves*, in Bifurcation Theory and Applications in Scientific Disciplines, O. Gurel and O. E. Rossler, eds., Ann. New York Acad. Sci., 316, pp. 263–278.

———(1984), *Bifurcation analysis of reaction-diffusion equations V. Rotating waves on a disc*, in Partial Differential Equations and Dynamical Systems, W. E. Fitzgibbon, ed., Res. Notes in Math., 101, Pitman, San Francisco, pp. 35–63.

V. BALAKOTAIAH (1987), *On the steady-state behavior of the autocatalator model $A+2B=3B$, $B=C$ in a stirred tank reactor*, Proc. Roy. Soc. London Ser. A, 411, pp. 193–206.

V. BALAKOTAIAH AND D. LUSS (1984), *Global analysis of the multiplicity features of multireaction lumped-parameter systems*, Chem. Eng. Sci., 39, pp. 865–881.

P. CHOSSAT AND M. GOLUBITSKY (1987), *Hopf bifurcation in the presence of symmetry, center manifold and Liapunov–Schmidt reductions*, in Oscillation, Bifurcation, and Chaos, F. V. Atkinson, W. F. Langford, and A. B. Mingarelli, eds., CMS Conf. Proc., 8, American Mathematical Society, Providence, RI.

P. CHOSSAT, M. GOLUBITSKY, AND B. KEYFITZ (1986), *Hopf–Hopf mode interactions with $O(2)$ symmetry*, Dynamics Stability Systems, 1, pp. 255–292.

R. CUSHMAN AND J. A. SANDERS (1986), *Nilpotent normal form and the representation theory of $sl(2, \mathbf{R})$*, in Multiparameter Bifurcation Theory, M. Golubitsky and J. Guckenheimer, eds., Contemp. Math., 56, American Mathematical Society, Providence, RI.

G. DANGELMAYR AND E. KNOBLOCH (1987), *The Takens–Bogdanov bifurcation with $O(2)$ symmetry*, Philos. Trans. Roy. Soc. London Ser. A, 322, pp. 243–279.

E. J. DOEDEL, A. D. JEPSON, AND H. B. KELLER (1984), *Numerical methods for Hopf bifurcation and continuation of periodic solution paths*, in Computing Methods in Applied Sciences and Engineering VI, R. Glowinski and J. L. Lions, eds., North-Holland, Amsterdam.

C. ELPHICK, M. MERON, AND E. A. SPIEGEL (1990), *Patterns of propagating pulses*, SIAM J. Appl. Math., 50, pp. 490–503.

C. ELPHICK, E. TIRAPEGUI, M. E. BRACHET, P. COULLET, AND G. IOOSS (1987), *A simple global characterization for normal forms of singular vector fields*, Physica, D, 29, pp. 95–127.

T. ERNEAUX AND M. HERSCHKOWITZ-KAUFMAN (1977), *Rotating waves as asymptotic solutions of a model chemical reaction*, J. Chem. Phys., 66, pp. 248–250.

——— (1978a), *Bifurcation diagram of a model chemical reaction* I. *Stability of time-periodic solutions*, Bull. Math. Biol., 41, pp. 21–38.

——— (1979b), *Bifurcation diagram of a model chemical reaction* II. *Two-dimensional time-periodic patterns*, Bull. Math. Biol., 41, pp. 767–790.

W. W. FARR (1986), *Mathematical modelling*: *Dynamics and multiplicity*, Ph.D. thesis, University of Minnesota, Minneapolis, MN.

W. W. FARR AND R. ARIS (1987), *Degenerate Hopf bifurcations in the* CSTR *with reactions $A \to B \to C$*, in Oscillations, Bifurcations, and Chaos, F. V. Atkinson, W. F. Langford, and A. B. Mingarelli, eds., CMS Conf. Proc., 8, American Mathematical Society, Providence, RI.

W. W. FARR, C. LI, I. S. LABOURIAU, AND W. F. LANGFORD (1989), *Degenerate Hopf bifurcation formulas and Hilbert's 16th problem*, SIAM J. Math. Anal., 20, pp. 13–30.

J. A. FEROE (1986), *Existence of traveling wave trains in nerve axon equations*, SIAM J. Appl. Math., 46, pp. 1079–1097.

R. FIELD AND M. BURGER (1985), *Oscillations and Traveling Waves in Chemical Systems*, John Wiley, New York.

S. A. VAN GILS AND J. MALLET-PARET (1984), *Hopf bifurcation and symmetry*: *Standing and traveling waves on a circle*, Proc. Roy. Soc. Edinburgh Sect. A, 104, pp. 279–307.

M. GOLUBITSKY AND W. F. LANGFORD (1981), *Classification and unfoldings of degenerate Hopf bifurcations*, Differential Equations, 41, pp. 375–415.

M. GOLUBITSKY AND M. ROBERTS (1987), *A classification of degenerate Hopf bifurcations with $O(2)$ symmetry*, J. Differential Equations, 69, pp. 216–264.

M. GOLUBITSKY AND D. G. SCHAEFFER (1985), *Singularities and Groups in Bifurcation Theory*, Vol. 1, Appl. Math. Sci., 51, Springer-Verlag, New York.

M. GOLUBITSKY AND I. STEWART (1985), *Hopf bifurcation in the presence of symmetry*, Arch. Rational Mech. Anal., 87, pp. 107–165.

M. GOLUBITSKY, I. STEWART, AND D. G. SCHAEFFER (1988), *Singularities and Groups in Bifurcation Theory*, Vol. 2, Appl. Math. Sci., 69, Springer-Verlag, New York.

P. GRAY AND S. K. SCOTT (1983), *Autocatalytic reactions in the isothermal, continuous stirred tank reactor, isolas and other forms of multistability*, Chem. Eng. Sci., 38, pp. 29–43.

——— (1985), *Sustained oscillations and other exotic patterns of behavior in isothermal reactions*, J. Phys. Chem., 89, pp. 22–32.

J. GUCKENHEIMER AND P. HOLMES (1983), *Nonlinear Oscillations, Dynamical systems, and Bifurcations of Vector Fields*, Appl. Math. Sci., 42, Springer-Verlag, New York.

D. HENRY (1981), *Geometric Theory of Semilinear Parabolic Equations*, Lecture Notes in Math., 840, Springer-Verlag, New York.

A. A. KIRILLOV (1976), *Elements of the Theory of Representations*, Grundlehren, 220, Springer-Verlag, Berlin.

I. S. LABOURIAU (1985), *Degenerate Hopf bifurcation and nerve impulse*, SIAM J. Math. Anal., 16, pp. 1121–1133.

——— (1989), *Degenerate Hopf bifurcation and nerve impulse, part* II, SIAM J. Math. Anal., 20, pp. 1–12.

N. LEVINSON AND R. M. REDHEFFER (1970), *Complex Variables*, Holden-Day, San Francisco.

K. MAGINU (1985), *Geometric characteristics associated with stability and bifurcations of periodic travelling waves in reaction-diffusion systems*, SIAM J. Appl. Math., 45, pp. 750–773.

J. MASELKO AND H. L. SWINNEY (1986), *Complex periodic oscillations in the Belousov–Zhabotinski reaction*, J. Chem. Phys., 85, pp. 6430–6441.

I. MELBOURNE, P. CHOSSAT, AND M. GOLUBITSKY (1988), *Heteroclinic cycles involving periodic solutions in mode interactions with $O(2)$ symmetry*, Proc. Roy. Soc. Edinburgh Sect. A, 113, pp. 315–345.

Z. NOSZTICZIUS, W. HORSTHEMKE, R. MCCORMICK, H. SWINNEY, AND W. Y. TAM (1987), *Sustained chemical waves in an annular gel reactor: A chemical pinwheel*, Nature, 329, pp. 619–620.

R. H. RAND AND D. C. ARMBRUSTER (1978), *Perturbation Methods, Bifurcation Theory and Computer Algebra*, Springer-Verlag, New York.

W. RUDIN (1973), *Functional Analysis*, McGraw-Hill, New York.

D. RUELLE (1973), *Bifurcations in the presence of a symmetry group*, Arch. Rational Mech. Anal., 51, pp. 136–152.

D. H. SATTINGER (1979), *Group Theoretic Methods in Bifurcation Theory*, Lecture Notes in Math., 762, Springer-Verlag, Berlin.

S. SCHECHTER (1976), *Bifurcation with symmetry*, in The Hopf Bifurcation and its Applications, J. E. Marsden and M. McCracken, eds., Appl. Math. Sci., 19, Springer-Verlag, New York.

S. K. SCOTT AND W. W. FARR (1988), *Dynamic fine structure in the cubic autocatalotor*, Chem. Eng. Sci., 43, pp. 1082–1087.

A. SPENCE AND A. D. JEPSON (1984), *The numerical calculation of cusps, bifurcation points and isola formation points in two parameter problems*, in Numerical Methods for Bifurcation Problems, T. Küpper and H. D. Mittelmann, eds., ISNM series, Birkhäuser, Basel.

W. TAM, W. HORSTHEMKE, Z. NOSZTICZIUS, AND H. L. SWINNEY (1988), *Sustained spiral waves in a continuously fed unstirred chemical reactor*, J. Chem. Phys., 88, pp. 3395–3396.

J. J. TYSON AND J. P. KEENER (1988), *Singular perturbation theory of travelling waves in excitable media (a review)*, Phys. D, 32, pp. 327–361.

A. T. WINFREE (1972), *Spiral waves of chemical activity*, Science, 175, pp. 634–636.